



Investigating the properties and microstructure of high-performance cement composites with nano-silica, silica fume, and ultra-fine TiO₂

Ashkan Saradar¹ · Yousof Rezakhani² · Komeil Rahmati¹ · Farzad Johari Majd³ · Mohammad Mohtasham Moein⁴ · Moses Karakouzian⁵

Received: 8 November 2023 / Accepted: 15 February 2024 / Published online: 5 March 2024
© Springer Nature Switzerland AG 2024

Abstract

Nanomaterials find widespread use in industries, including construction, due to their superior mechanical, thermal, and electrical characteristics. Addressing cement composites' weaknesses like low tensile strength and brittleness, researchers increasingly use supplementary cementitious materials and nanoparticles. This study investigates the effects of varied proportions of silica fume (SF), nano-silica (nS), and ultra-fine TiO₂ (UFTiO₂) in both mixed and separate phases on cement composites. SF represents the pozzolanic family, while nS and UFTiO₂ stand for nanomaterials. Tests measured compressive, flexural, and impact strengths, abrasion resistance, and electrical resistivity. Scanning electron microscopy examined microstructure-property relationships. SF and nS enhanced the mechanical strength of the composites, with SF proving superior in durability. The addition of UFTiO₂ increased the compressive strength slightly for SF samples (4–7%) and more for nS samples (8–14%). SF samples with UFTiO₂ showed 16–25% more flexural strength than nS samples with UFTiO₂. The addition of UFTiO₂ also raised the electrical resistance by 24–30% for nS samples and 14.5–31.5% for SF samples after 14 days. UFTiO₂ affected the abrasion resistance significantly, exhibiting diverse roles in nS and SF specimens. The first crack strength and failure strength for the mixtures containing SF were in the range of 33–36 blows and 39–43 blows, respectively. Meanwhile, for the mixtures containing nS, this impact range was reduced to a maximum of 57%. The impact test results followed the two-parameter Weibull distribution well, with an R^2 value exceeding 0.891 across concrete mixes. The study demonstrates the potential of nanomaterials to improve the performance of cement composites for various applications.

Keywords Nanomaterial · Nano-silica · Silica fume · Nano-titanium dioxide · Mechanical properties · Microstructure · Impact strength

✉ Komeil Rahmati
komeil_rahmati@msc.guilan.ac.ir

Ashkan Saradar
ashkan.saradar@gmail.com

Yousof Rezakhani
yousofrezakhani@gmail.com

Farzad Johari Majd
farzad.johari1985@gmail.com

Mohammad Mohtasham Moein
m.mohtasham.moein@gmail.com

Moses Karakouzian
mkar@unlv.nevada.edu

¹ Department of Civil Engineering, University of Guilan, Rasht, Iran

² Department of Civil Engineering, Pardis Branch, Islamic Azad University, Pardis, Iran

³ Kadous Institute of Higher Education, Rasht, Iran

⁴ Department of Civil Engineering, Allameh Mohaddes Nouri University, Nour, Mazandaran, Iran

⁵ Department of Civil and Environmental Engineering and Construction, University of Nevada, Las Vegas, NV, USA

Introduction

Cement mortar (CM) is a widely used building material, which is used in various fields such as masonry foundation walls, load-bearing exterior masonry walls, and masonry footings. CM usually has good compressive strength and resistance to fire [1, 2], but its weak point can be its low resistance against flexure, tension, and impact [3–6]. Like concrete, one of the main components of CM is cement, which is responsible for the production of 5–7% of CO₂ on the planet [7–12]. Estimates indicate that by 2050, the demand for Portland cement will increase by 200% compared to the rate of 2010 [13]. On the other hand, emerging nanotechnology has created a new window to improve and enhance the properties of various materials. This technology is the meeting point of thought and action of scientists and researchers of various disciplines and a key component of this century's technical progress [14–16]. In 1959, the idea of nanotechnology was proposed by Richard Feynman during a speech entitled, "Plenty of Room at the Bottom" [17–19]. His theory stated the possibility of direct manipulation and arrangement of molecules and atoms in the near future. The technical committee of RILEM in a report entitled TC 197-NCM has investigated the use of nanoparticles to improve the durability and mechanical characteristics of cement composites [20]. Nanotechnology studies the properties of materials smaller than 100 nm and their usage. Because the properties of concrete and CM are due to their structure in nano-dimensions, there are hopes for the use of nanotechnology in improving concrete's mechanical properties (such as compressive strength, tensile strength, impact strength, modulus of elasticity, creep, and shrinkage) and durability properties (such as durability against the chemical attacks of sulfates and chlorine ions, durability against the cycle of thawing and freezing, and durability against the phenomenon of carbonation). As shown in Fig. 1, nanotechnology has made significant advances in recent years.

Nano-silica (nS) is used in construction applications. The nS present in concrete and CM reacts with lime during cement hydration, and C–S–H gel is formed after this reaction, which leads to improving concrete's mechanical properties and durability [21]. According to a review study by Mohtasham Moein et al. [22], nS enhanced 15 key properties of concrete, namely: (1) slump, (2) compressive strength, (3) flexural strength, (4) tensile strength, (5) impact strength, (6) water absorption, (7) chloride penetration, (8) carbonation, (9) acid attack, (10) sulfate attack, (11) freeze and thaw, (12) electrical resistivity, (13) elevated temperature, (14) shrinkage, and (15) microstructure. In some research, it was observed that the use of nS increases the packing of particles [23]. In addition, the

presence of nS can improve the hydration rate of cement, which in turn lowers the dormant period and time of setting [24]. Another advantage of nS is that it can reduce the porosity of concrete and create a denser surface transfer zone and also prevent degradation [25, 26]. The use of nS can also be an effective factor to reduce CO₂ from concrete products, and it can provide more affordable concrete [27, 28].

Nano-TiO₂ (UFTiO₂) is a semiconducting photocatalyst, which can create self-cleaning properties. UFTiO₂ is a useful material present in a wide range of materials. For example, UFTiO₂ is used in paints, glasses, cosmetics, cement, wallpaper materials, and ceramics [29, 30]. Concrete and CM containing these nanoparticles are safe from the adverse effects of sunlight and pollution. Also, UFTiO₂ in the pavement field can be an effective factor in gas decomposition caused by vehicles [31, 32]. In general, UFTiO₂ enables the photocatalytic degradation of pollutants (such as VOCs, CO, NO_x, aldehydes, and chlorophenols) [33]. The UFTiO₂ is an engineered material that has the potential for a unique beneficial reaction with an external stimulus [34]. Minimizing the number and refinement of these pores' sizes can greatly increase the structures' service life. The UFTiO₂ is used as a material with a high surface area that can be used as filler. The surface of these particles facilitates the formation of Ca(OH)₂, and on the other hand, it is the place of C–S–H nucleation. Thus, decreasing the porosity of the matrix may lead to less permeable concrete, which significantly affects the structure's serviceability.

Figure 2 shows the hydration reaction models of mixtures without and containing nanomaterials (nS and UFTiO₂). C–S–H seeds are obtained from the adhesion of nanoparticles to the cement paste in the early ages, and then C–S–H gel is gradually obtained [35]. During the hydration reaction, nano-silica (nS), by consuming Ca⁺², causes the formation of C–S–H seeds. The hydration process is therefore accelerated through the seeding process. By consuming C₂S and C₃S by nS, higher amounts of C–S–H and CH gel are produced. CH can also undergo a pozzolanic reaction with nS, which can reduce CH in the next steps. The nS is able to reduce the porosity of C–S–H gel by its function [36]. The reduction of harmful pores by nS can be because nS provides the basis for the formation of ettringite with a more network structure between cement particles. The hydration rate of cement in the presence of nano-titanium oxide (UFTiO₂) improves to some extent, but it is less powerful compared to other nanomaterials in this field [32]. The ability of nucleation effect from UFTiO₂ is not favorable, and this can be due to the lower tendency of UFTiO₂ to consume C₂S and C₃S [37]. In addition, the presence of UFTiO₂ can slow down the precipitation of CH, which brings an increase in porosity

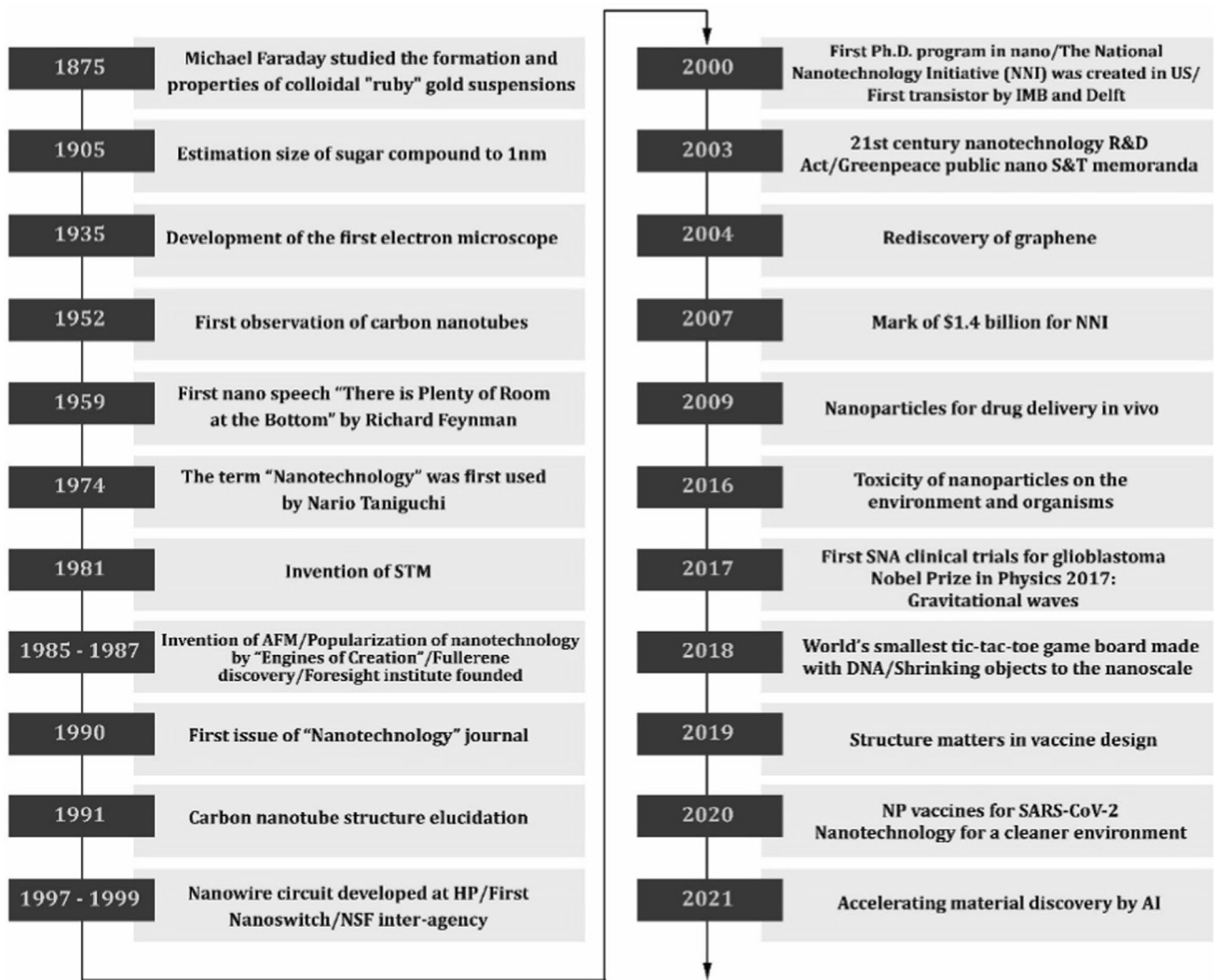


Fig. 1 Timeline of nanotechnology progress

at the age of 1 day [38], but with the passage of time and the deposition of $UFTiO_2$, the density of the cement paste increases due to the seeding and filling properties.

One of the side products of the ferrosilicon and silicon industry is silica fume (SF). The size of silica fume particles is such that more than 95% of them are smaller than 1 μ m. The shape of silica soot particles is spherical and has a large percentage of amorphous silicon dioxide, and small amounts of magnesium, iron, and alkali oxides [39–43]. We can mention the following benefits of using silica fume in concrete [40, 44, 45]: (1) increased toughness, (2) improved durability, (3) increased abrasion resistance, (4) high compressive strength at early ages, (5) improved tensile strength, (6) improved flexural resistance, (7) very low permeability against chloride and water penetration, and (8) improved electrical resistance.

Significance of the investigation

This study was designed to investigate the behavior of CM containing nanomaterials and pozzolans in separate and combined use. From the family of nanomaterials, nS (due to high popularity) and $UFTiO_2$ (due to few studies) were chosen, as well as from the family of pozzolans SF (due to high popularity). Table 1 shows the existing gaps regarding the materials considered for CM. Although many studies have been conducted on the impact strength of concretes containing SF and nS, no studies have been conducted on CM containing these types of materials. This test is important for these reasons: (1) Concrete elements are exposed to short-term dynamic loads during their service life (including shocks caused by earthquakes, bullets,

Fig. 2 Hydration reaction models

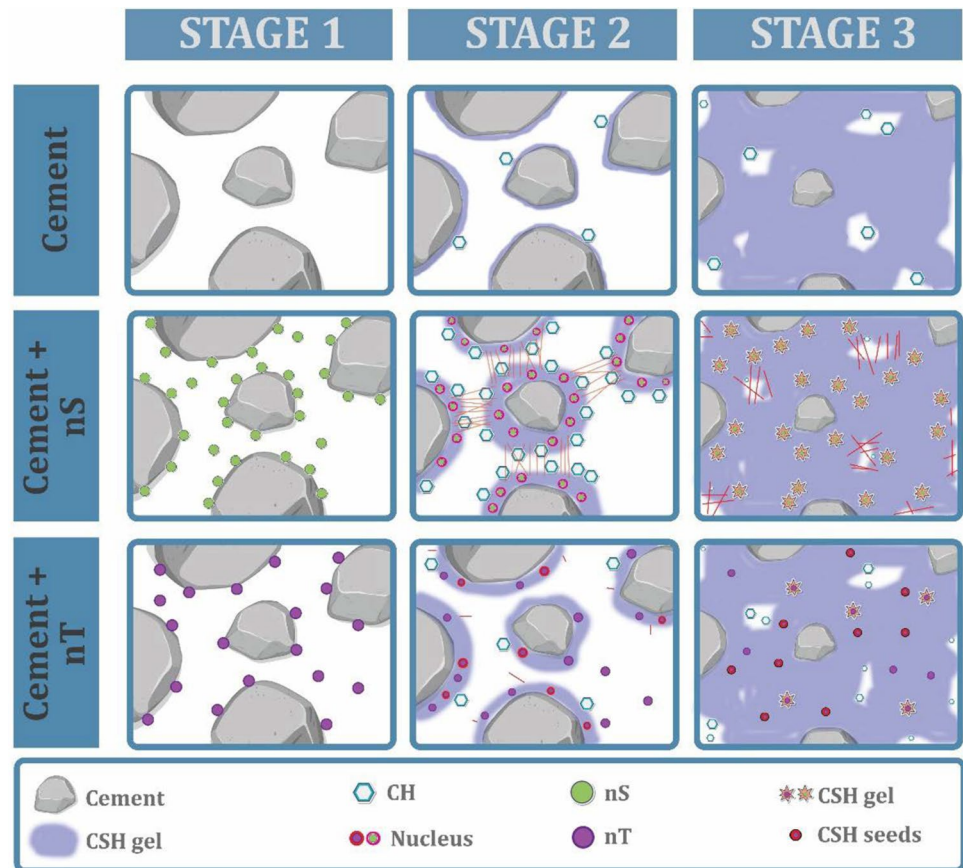


Table 1 Items reviewed and not reviewed by researchers on the subject

Type of composition	Additives	Compressive	Flexural	Electrical	Abrasion	Impact	SEM
Separate use	Silica Fume (SF)	[46]	[47]	[48]	[49]	×	[50]
	Nano-silica (nS)	[51]	[52]	[53]	[47]	×	[53]
Combined use	SF + UFTiO ₂	×	×	×	×	×	×
	nS + UFTiO ₂	×	×	×	×	×	×

missiles, etc.), and (2) the type of behavior of concrete elements against loads short-term dynamic is completely different from a static state. Also, a two-parameter Weibull distribution was used to analyze the data obtained from the impact test. According to Table 1, for the combined phase of materials (SF + UFTiO₂ and nS + UFTiO₂) no study has been done by other researchers. In general, the objectives of this study include: (1) investigating the mechanical characteristics and durability of CM containing nanomaterial and pozzolan (in separate and combined phases), (2) investigating the impact behavior of CM (using two-parameter Weibull distribution), (3) micrographs investigation in order to find the relationship between the microstructure and properties of cement mortars containing nano-silica, silica Fume, and UFTiO₂. In other words, using pozzolanic additives and nanomaterials to improve the characteristics of CMs toward eco-friendly

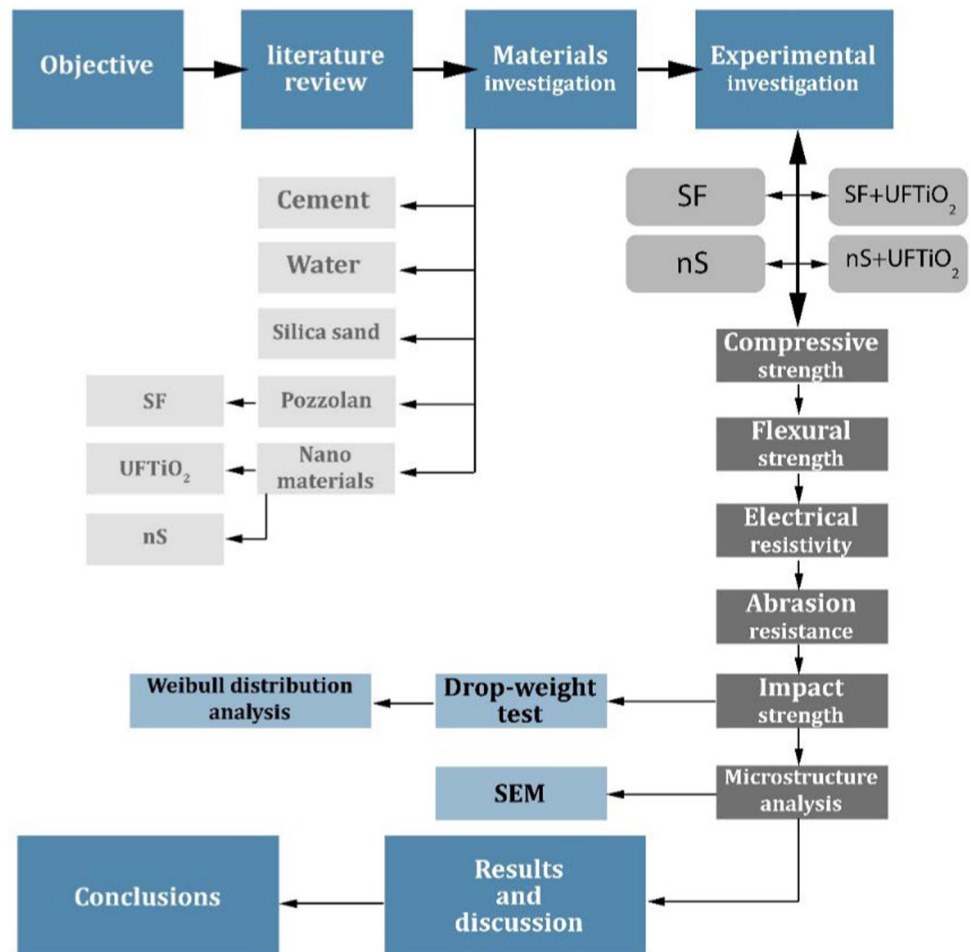
construction materials and reducing the cement content while preserving mechanical properties of the CMs are the main objective of the present study. The methodology of this study is shown in Fig. 3.

Research background

In recent years, various studies have investigated the separate use of SF or nS in cement mortars, but there are still tests such as impact tests that have not been addressed. Also, the use of SF or nS in combination with other materials (both pozzolanic and nanomaterials) has been investigated, with the difference that the combination of these materials with UFTiO₂ in cement mortars has not been investigated.

Gesoglu et al. [54] studied the mechanical properties of ultra-high-performance concrete mixtures containing nS and

Fig. 3 Methodology



SF which were evaluated. The results show that incorporating 2% nS by cement weight is optimum with the highest compressive strength. In a study by Nili and Ehsani [55], ternary cementitious composites containing nS and SF show high compressive strength, which then was related to the dense matrix and ITZ induced by these particles. The SEM micrographs show no observable porosity at the ITZ. Research shows that for replacement values below 2%, the addition of nS improves the properties of cement composites [56–58].

In general, studies conducted with the aim of investigating the role of UFTiO₂ in cement composites show improved properties. An experimental study on the physical properties of nano-UFTiO₂-containing cement composites by Li et al. [59] reveals that the abrasion resistance of the composite improves in the presence of nano-UFTiO₂. Diffusion of chloride and scouring are the two most important causes of deterioration in marine environments, and a study carried out by Li et al. [60] shows that UFTiO₂ can positively affect the microstructure of cement composites and reduce the porosity so that both chloride diffusion and scouring can be minimized. Rao et al. [61] added nano-UFTiO₂ and

nS to self-compacting mixtures and observed that in high concentrations of nS, mechanical strengths, especially flexural strength, decreased while the composite’s water absorption increased. By using nano-UFTiO₂ and nS in recycled-aggregate concrete, Ying et al. [62] reduced the diffusion of chloride ions, which stems from the pore refinement phenomenon induced by nanoparticles. More research about the addition of nano-TiO₂ resulted in a better performance compared to that of plain concrete [62, 63].

The capabilities of SF caused researchers to conduct numerous studies on its application in the construction industry. Karthikeyan et al. [64] improved the compressive strength of concrete by adding silica fume in conjunction with ultra-fine TiO₂. Madani et al. [65] suggest a replacement value of at least 3% for SF to obtain the optimum mix design for eco-friendly concretes made with silica fume and Pumice. Studies by Pedro et al. [66] and Mastali and Dalvand [67] examine the use of SF as a partial replacement for cement in HPC and self-compacting concrete, respectively. Several studies have examined the effect of SF on various properties of concrete. Song et al. [68], Ali et al. [69], and Lin et al. [70] investigated the permeability of SF concrete.

Siddique [40], Singh et al. [71], and Mansoori et al. [12] discussed the water absorption of SF concrete. Mazloom et al. [72], Tanyildizi et al. [73], Saradar et al. [43], and Wu et al. [74] conducted studies on the compressive strength of SF concrete. The results of using various percentages of SF in prior studies are briefly reported in Table 2.

Experimental program

Materials

The cement used in this study was Type I-42.5, produced by Hegmatan Cement factory, which met the standard specifications of ASTM-C150 [75]. The specific gravity and fineness of the cement were 3.15 and 3250 cm²/g, respectively. Silica fume, produced by Shimisakhteman company, was used as a partial replacement for cement in mixed proportions. The silica fume met the standard specifications of ASTM-C1240 [76]. Table 3 shows the chemical composition of silica fume and cement. Silica sand, supplied by Parsilis company, was used as fine aggregates. The silica sand passed sieve number 30 (smaller than 600 microns) according to ASTM C778 [77]. Polycarboxylate-based superplasticizer, produced by Shimisakhteman company, was used as a water-reducing agent and retarder. The superplasticizer met the standard specifications of ASTM-C494 [78]. Ultra-fine TiO₂, supplied by Notrino company, was used in mixed proportions. The diameter of the TiO₂ particles was about 200 nm. Nano-silica, supplied by Isatis Yazd company, was used in this study. The diameter of the nano-silica particles was about 15 nm. Table 4 presents the properties of nano-silica and UFTiO₂.

Mix designs

Fabricating, molding, and curing were performed in accordance with the requirements of the ASTM C109 [79] test method. First, cementitious materials including cement and silica fume (if applicable) or nano-silica (if applicable) were mixed for about one minute to gain a homogenous mixture of dry materials. Then, the silica sand was added, and the mixing continued for another two minutes. UFTiO₂ was added gradually to the dry mix and the mixing proceeded at a high speed. The blend of water and superplasticizer was added at the end, and the speed of mixing was slowed for about one minute until the paste formed. Finally, one-minute mixing was performed at a high speed. The slump flow measure for all mixtures is maintained under 110 ± 10 mm. Figure 4 shows the timeline of making the mixtures. SF and nS for their pozzolanic reactions and UFTiO₂ for its participation in hydration reactions were considered as cementitious materials. In all mix designs, the water-to-cementitious

material ratio (W/CM) was considered constant (0.38) to prevent the loss of mechanical strength, which occurs as a result of increasing the ratio. In all mix designs, the water-to-cementitious material ratio was considered constant to prevent the loss of mechanical strength, which occurs as a result of increasing the ratio. Moreover, keeping this ratio constant would simplify the industrial application and provide enough water molecules for secondary reactions alongside the hydration such as pozzolanic reactions of SF and nS. According to the use of different cementitious materials (silica fume and nano-silica) and TiO₂ in mix proportions, however, to obtain mixtures with desirable workability, a superplasticizer was added in different volume percentages. After the mixing procedure and slump flow test, the prepared fresh mixture was poured into molds in three layers. Each layer of fresh mixture was compacted by the standard rod through pounding for 32 times. Finally, the surface of the mold flattened with spatula and covered by plastic sheets and kept in moist room in standard lab conditions for 24 h. After 24 h, the samples were removed from the mold and placed in water for curing (23 ± 1 °C). Table 5 shows the composition characteristics of mixed designs of this study. A total of 54 cubes (50 mm edges), 54 prisms (40 mm × 40 mm × 160 mm), 72 cylinders (200 mm × 100 mm), 18 plates (100 mm × 100 mm × 20 mm), and 12 cylinders (150 mm × 300 mm) were prepared in this study.

Replacing cement with additives such as silica fume considering the environmental impact of both materials (cement as a major source of CO₂ and silica fume as an industrial by-product), the replacement of cement and reducing its content in cement composites while maintaining or improving characteristics of the mixtures could help reduce total eCO₂ of the mixture [80, 81]. Furthermore, nanomaterials such as nS can significantly improve the mechanical and physical properties of the CMs which supersedes the drawback of environmental issues associated with nanomaterials [22]. UFTiO₂ plays more than mechanical improvement on CMs and has pollution treatment benefits which beside the reduction of eCO₂ can add functional values like self-cleaning properties to the surface of this composites [82, 83].

Tests

Figure 5 shows a complete description of this study's experiments and details. The tests considered in this study include (1) compressive strength, (2) flexural strength, (3) electrical resistivity (4) abrasion resistance, (5) impact strength, and (6) Microstructure analysis.

Compressive strength

The test was performed based on the ASTM-C109 [79]. The compressive strength of cubic specimens with 50 mm × 50

Table 2 A brief report on the effect of using silica fume in prior studies

Ref	Replace-ment Of SF (%)	Other additives	Tests	Results
[65]	3, 6, 9	Pumice	Slump, compressive strength, Rapid chloride migration, capillary water absorption, SEM	Significant improvement in durability at 90 days./Compressive strength of 365 days of the mixed mixture 60% pumice + 9% silica fume = 75 MPa /Introducing silica fume as a pumice supplement. /It is recommended to use at least 3% silica fume to provide excellent performance in increasing durability and mechanical properties
[66]	5, 10	Fly ash Recycled aggregates	Compressive strength, tensile strength, modulus of elasticity, Water absorption, UPV, chloride penetration, Carbonation resistance	It was mentioned that the densification process used in silica fume causes the formation of agglomerates, which reduces the performance of concrete
[67]	7, 14	Steel fiber (0.25, 0.5, 0.75%)	Compressive strength, tensile strength, flexural strength, impact strength	A higher dose of SF resulted in a lower slump flow diameter./Mixtures containing SF and 0.75% steel fibers exhibited the highest compressive, tensile, and bending strength. /These control mixtures containing SF and the mixture containing SF and 0.75% steel fibers showed the highest impact strength, measured by first crack strength and fracture strength
[72]	6, 10, 15	---	Slump, Compressive strength, Elastic modulus, Shrinkage, Creep,	Workability decreased as the dosage of SF increased. /Short-term mechanical properties (compressive strength and modulus) improved with the increase in the dosage of SF. /Total shrinkage was not significantly affected by the use of SF. /Autogenous shrinkage increased with the increase in SF. /Basic creep decreased as SF increased. /The amount of expansion decreased with the increase in SF
[73]	10, 20, 30	Pumice	Under different temperatures (20, 200, 400, and 800 °C): Compressive strength, tensile strength	The mixture containing 20% SF showed the best compressive and tensile strength results across different temperatures. /The addition of SF mitigated the decrease in compressive and tensile strength at high temperatures

Table 3 Chemical characteristics of cement and silica fume

Compound	Cement (%)	Silica fume (%)
CaO	64.38	1.87
SiO ₂	21.08	89.22
Al ₂ O ₃	5.36	1.2
Fe ₂ O ₃	3.64	2.12
MgO	2	1.61
K ₂ O	0.82	1.056
Na ₂ O	0.5	0.556
L.O.I (Loss On Ignition)	0.9	2.6

Table 4 The properties of nano-silica and UFTiO₂

	Diameter (nm)	Surface area (m ² /g)	Density (g/cm ³)	LOI (%)
nano-silica (nS)	15 ± 2	190 ± 25	2.3	≤ 1
UFTiO ₂	200–300	9	3.9	≤ 1

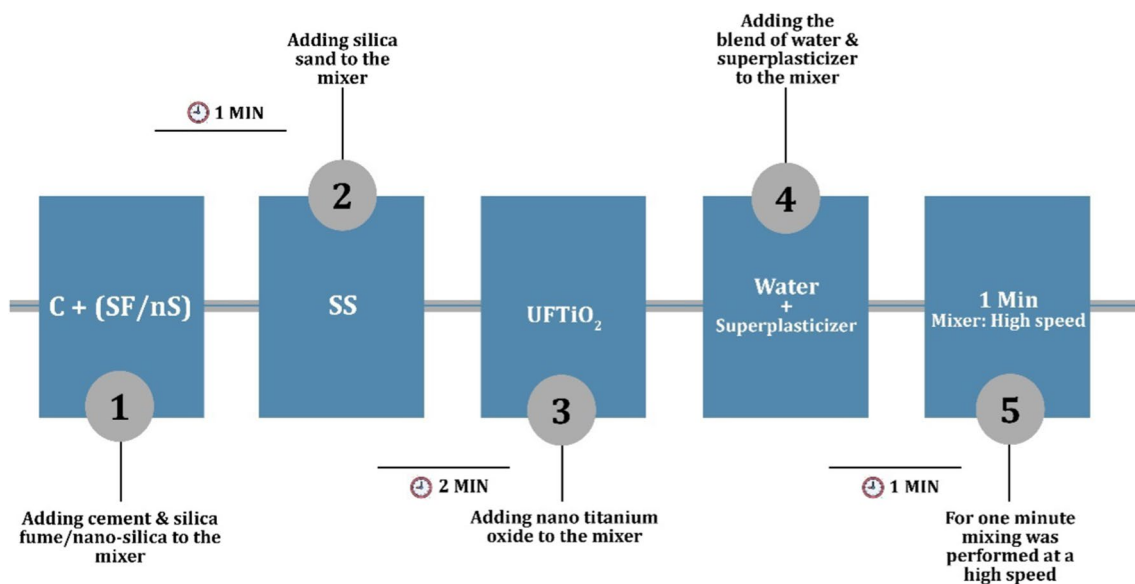
mm × 50 mm dimensions was measured at different ages (28, 56 and 90 days). In order to achieve reliable data on compressive strength of mixtures, three tests performed for each mixtures and age of testing. The average of the three tests was calculated and reported in compliance with the standard.

Flexural strength

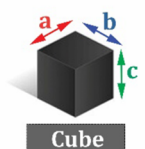
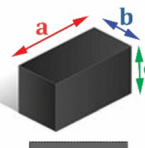
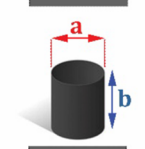
According to ASTM-C348 [84], the three-point bending test was used to measure the flexural strength of the prisms (40 mm × 40 mm × 160 mm). The test was conducted on three specimens per mix design at 28, 56, and 90 days, and the average results were reported. The loading area span length and the loading rate were 140 mm and 2 mm/min, respectively.

Electrical resistivity

This test was performed according to AASHTO TP 119 [85]. Since the result of the electrical resistivity measurement is

**Fig. 4** Timeline of making the mixtures**Table 5** Mix designs

N.O	Mix code	Cement (kg/m ³)	Silica sand (kg/m ³)	Silica fume (SF) (kg/m ³)	Nano-silica (nS) (kg/m ³)	UFTiO ₂ (kg/m ³)	W/b
1	SFT0	800	640	160	–	–	365
2	SFT2.5	800	620	160	–	20	372
3	SFT5	800	600	160	–	40	380
4	ST0	800	776	–	24	0	313
5	ST2.5	800	756	–	24	20	321
6	ST5	800	736	–	24	40	328

Tests	Standard	Curing time days	Shape	Dimension mm	
Compressive strength	ASTM-C109	28, 56, 90	Cube	a b c 50 50 50	
Flexural strength	ASTM-C348	28, 56, 90	Prism	160 40 40	
Electrical resistivity	ASTM-C348	14, 28, 56, 90	Cylinder	100 200	
Abrasion resistance	ASTM-C944	28	Cube	100 100 20	
Impact strength	ACI-544	28	Cylinder	150 300	

Microstructure analysis → Scanning Electron Microscopy (SEM)

Fig. 5 Description of tests and details

highly dependent on the amount of water present, ion concentration of pore solution, and porosity of the composite, this test can be a decisive criterion for the durability of the concrete structures. There are two conventional methods for determining the electrical resistivity values of cement composites called the two-probe and four-probe (Wenner) methods. Both methods have been used frequently by investigators in the field [86–89]. Both methods have their own advantages and disadvantages [90, 91]; nonetheless, both are the most reliable methods used to investigate the electrical resistivity of cement composites. In this research, to measure the bulk resistivity of the specimens, the two-probe method was used. The electrodes were attached to two opposite sides of each prismatic specimen in a way that the specimen was sandwiched between the electrodes. The applied and measured voltage and current were recorded, and the specific electrical resistivity of the specimens was calculated using Eq. (1).

$$R = (V/I) \times (A/L) \tag{1}$$

Abrasion resistance

The test was performed based on the standards of the ASTM-C944 [92] test method. Since the standard states that the specimens can be in any shape and size, the specimens with dimensions of 100 mm × 100 mm × 20 mm were fabricated so that they can be accommodated by the abrasion device. After removing from the water tank, the specimens were air-dried and the surface was cleaned with a cloth, first the weight of the specimen measured with a scale possessing the accuracy of 0.1 g, and then, the test was done in a 2-min

period. After determining the initial mass of a specimen, it was fastened in the abrasion device and the rotating cutter was mounted on the surface of the specimen. In 2-min increments, the surface of the specimen was cleaned with a brush and weighed with scale to measure the mass loss during each increment. The test was carried out on three different surfaces of specimens to gain an average of the mass loss of a specific mix design. Because of the mass loss measuring technique, the pure differential loss was calculated so the initial weight of the specimens was irrelevant.

Impact strength (drop-weight test)

Blast tests and projectile impact tests are methods for evaluating high-velocity impact tests [93–97]. The instrumented falling impact, the Charpy pendulum, and drop-weight tests are methods for conducting low-velocity impact tests [98–101]. The drop-weight test was performed according to the recommendation of the ACI 544 [102] committee. Figure 6 shows a schematic view of the drop-weight test device. The steel ball with a diameter of 63.5 mm is placed in the center of the upper surface of the disk. Then, repeated blows by a hammer weighing 4.45 kg from a height of 457 mm are applied to the disk. The two important items of this test include (1) first crack strength and (2) failure strength. The resistance of the first crack is recorded when the first crack is seen on the disk surface after repeated blows. After recording the first crack strength, the blows continue until the disk touches 3 of the metal lugs around it, in which case, the failure strength is recorded. The disk placed in the impact device has a thickness of 64 mm and a diameter of 150 mm, which is cut from a cylindrical sample of 300 mm × 150 mm. In

Fig. 6 Impact device specifications

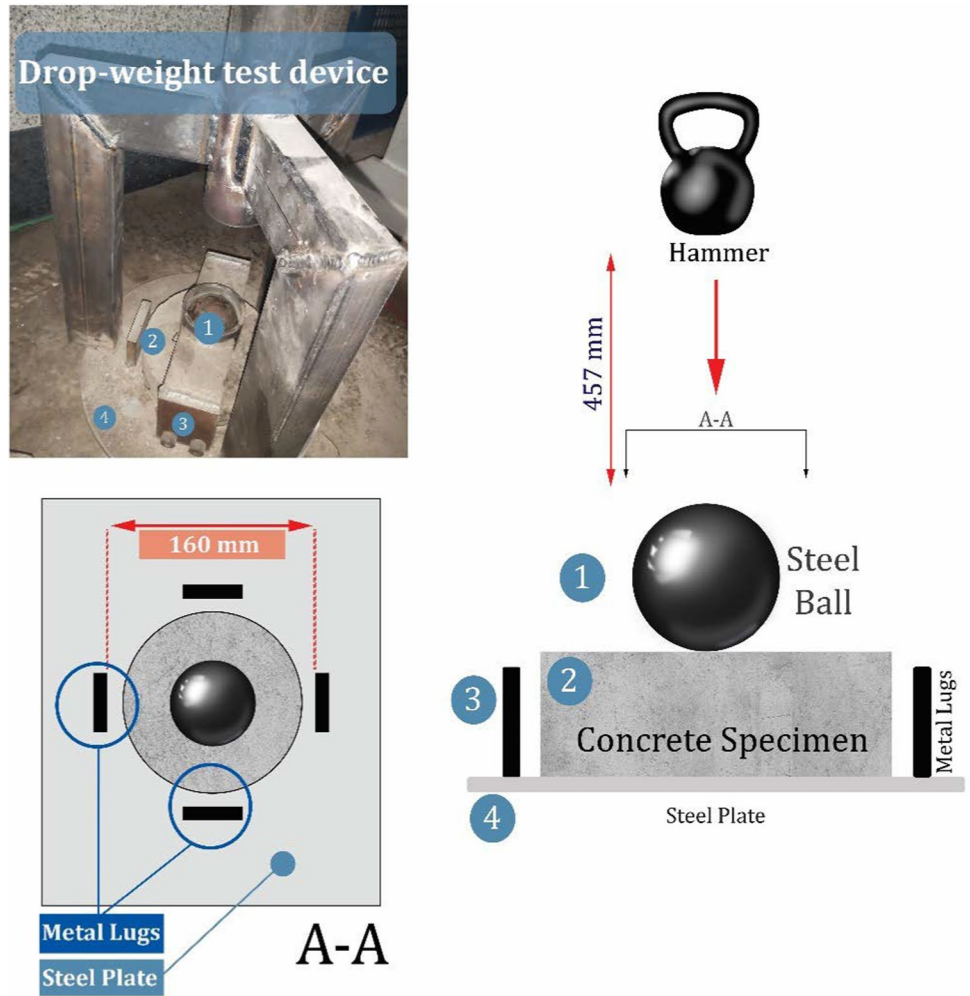
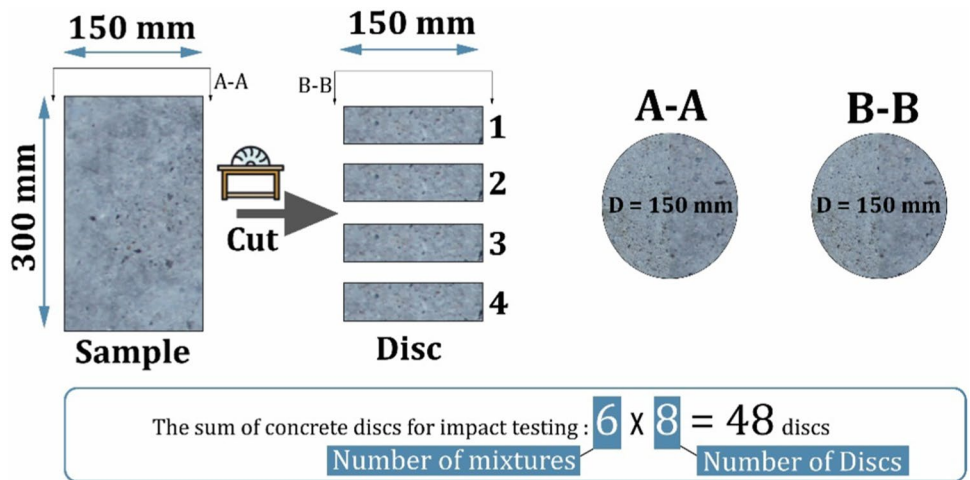


Fig. 7 Description of the size and number of samples and disks



this study, 2 cylindrical samples were considered, and a total of 8 disks were obtained for each mixture. Figure 7 shows a schematic view of the samples' dimensions and the number of disks.

Results and discussion

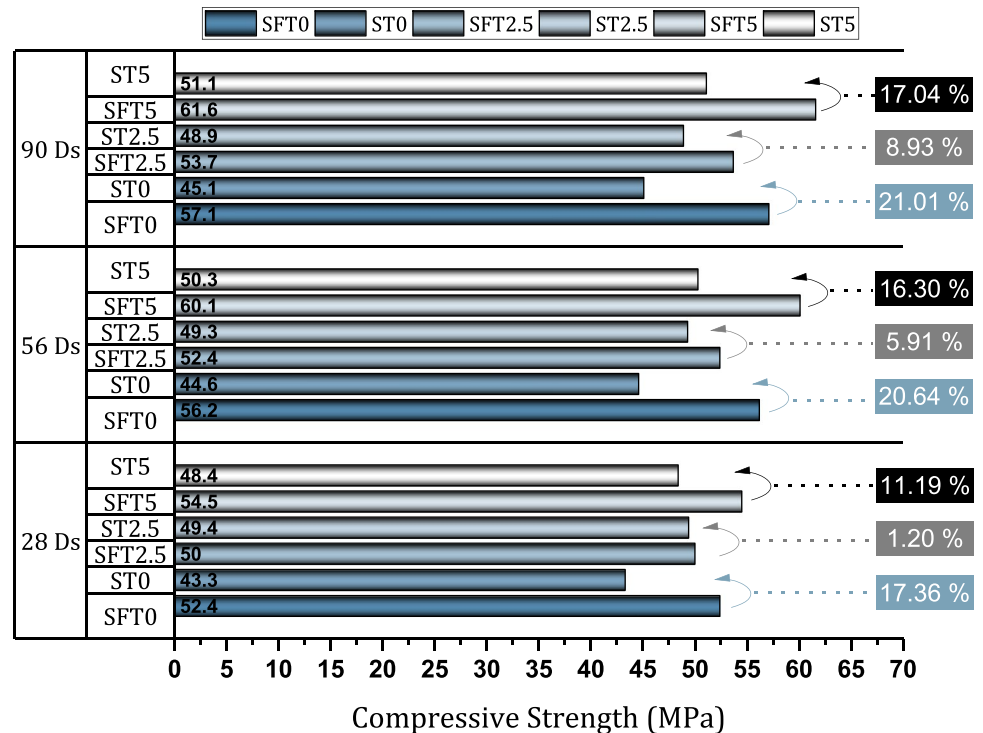
Compressive strength

Figure 8 shows the results of the compressive strength of different joints at the ages of 28, 56, and 90 days. The comparison of separate phase mixtures (SFT0 and ST0) shows that SF mixtures have higher compressive strength than samples containing nS. In this regard, the SFT0 mixture presents 21%, 1.2%, and 12.6% more than the ST0 mixture at the age of 28, 56, and 90 days, respectively. This superiority of SF can be attributed to its particle size distribution. The size of the SF particles is in the range of 100–500 nm. This wide range of the particles' diameter leads to a better reaction with the cement grains in different sizes and facilitates the moisture distribution inside the matrix. More complete hydration resulted, which in turn lowers the porosity and increases the strength. On the other hand, nS particles are all the same size, and due to their fineness and high reactivity, they chemically react with the very fine cement grains, but coarse grains remain non-hydrated or semi-hydrated. When a great number of nano-silica particles agglomerate, their reaction with the lime of cement is delayed, and a considerable amount of water may be confined around this mass of particles and the porosity increases [21, 103]. The weak zone around agglomerated particles could be a zone for the formation of microcracks and eventually lead to the specimen's

failure. The lack of CSH growth in the areas of agglomeration and porous media of the area allows the accumulation of water molecules and formation of silicic acid which can initiate the chemical reactions and expansion (local stress) in this area. The forces generated by reactions eventually deteriorate the CSH structures and initiate microcracks [104–106].

The examination of mixtures containing UFTiO₂ at the age of 28 days shows that the compressive strength of the ST2.5 mixture has increased by about 14% compared to ST0 (10.5% at the age of 56 days and 8.5% at the age of 90 days). In addition, the comparison of the ST5 mixture with the ST0 mixture shows that the compressive strength increased by 11.77%, 12.78%, and 13.30% at the ages of 28, 56, and 90 days, respectively. Along with the very fine particles of nS, UFTiO₂ particles enhance the packing density of the dry particles inside the specimen, which reduces the total capillary voids of the matrix. The high specific surface area of UFTiO₂ particles provides sufficient space for the nucleation of C–S–H and also for the formation of Ca(OH)₂ crystals. Following the mentioned hypothesis, other possibility can be discussed about the role of UFTiO₂ particles, which relates to free surface electrons of these particles and the facilitation CSH layers interconnection. The bonding of CSH gel among empty spaces of aggregates and improving binder quality of cementitious matrix with aggregates is another path to further improve the mechanical properties of CMs without participating in chemical reactions. In other words,

Fig. 8 Compressive strength results (28, 56, 90 days)



it appears that UFTiO_2 particles act as a mediator for development and attachment of CSH structures.

The addition of UFTiO_2 to the specimen containing SF has led to a slight increase in compressive strength. The reason for this contradictory behavior of UFTiO_2 in nS and SF mixtures might be that the addition of nS and UFTiO_2 significantly affects the packing density of particles, while in SF-containing specimens, this effect is not comparably significant. In other words, wide-range particle distribution of SF increases compaction to a level that UFTiO_2 particles nevertheless of their contribution to filling the voids, have less effect to bond the evolutionized CSH layers. This hypothesis is supported by few studies [107–109]. The results of compressive strength at 56 days show no significant increase in nS-containing specimens. This can be attributed to these particles' high reactivity and fineness, which greatly facilitates the hydration process at early ages. It is assumed that for up to 7 days, the full hydration of nS and cement is achieved. On the contrary, the growth of strength between the ages of 28 and 56 days is more considered in the specimens containing SF. The gelling process of coarser SF particles in the vicinity of Anhydrate C3S particles of cement owing to the reaction equilibrium ($2\text{S} + 3\text{CH} \rightarrow \text{C}_3\text{S}_2\text{H}_3$) affects the essential CSH production between these ages [110]. Although the reactivity of SF is much higher than other supplementary cementing

materials, the coarser size of SF particles compared to nS leads to hydration progress for longer periods. At 90 days, no significant increase is observed in either nS or SF-containing specimens. Due to their high reactivity, rapidly increasing the compressive strength at early ages seems to cause the specimens with nS to reach their full strength at 28 days, and the specimens containing SF reach the maximum strength at 56 days. Figure 9 shows the correlation between the compressive strength results of different ages of the mixtures. Examining the results of R^2 shows that there is an acceptable correlation between the compressive strength results of 28, 56, and 90 days. The coefficients derived from correlation lines indicate the impact of age on compressive strength growth and the predictability of the results based on interpolation. The R^2 value indicates how much of the data variation is explained by the regression model, from 0 (none) to 1 (all). In concrete analyses, R^2 values are often used to assess how well regression models can predict concrete properties or behavior from experimental or test data [111, 112]. The R^2 value of the regression model helps engineers and researchers to judge the fit of the model to the observed data. A high R^2 value means that the model reflects the relationship between the predictor variables and the concrete properties well. A low R^2 value shows that the model does not account for the data variation well and may need more refinement or alternative models.

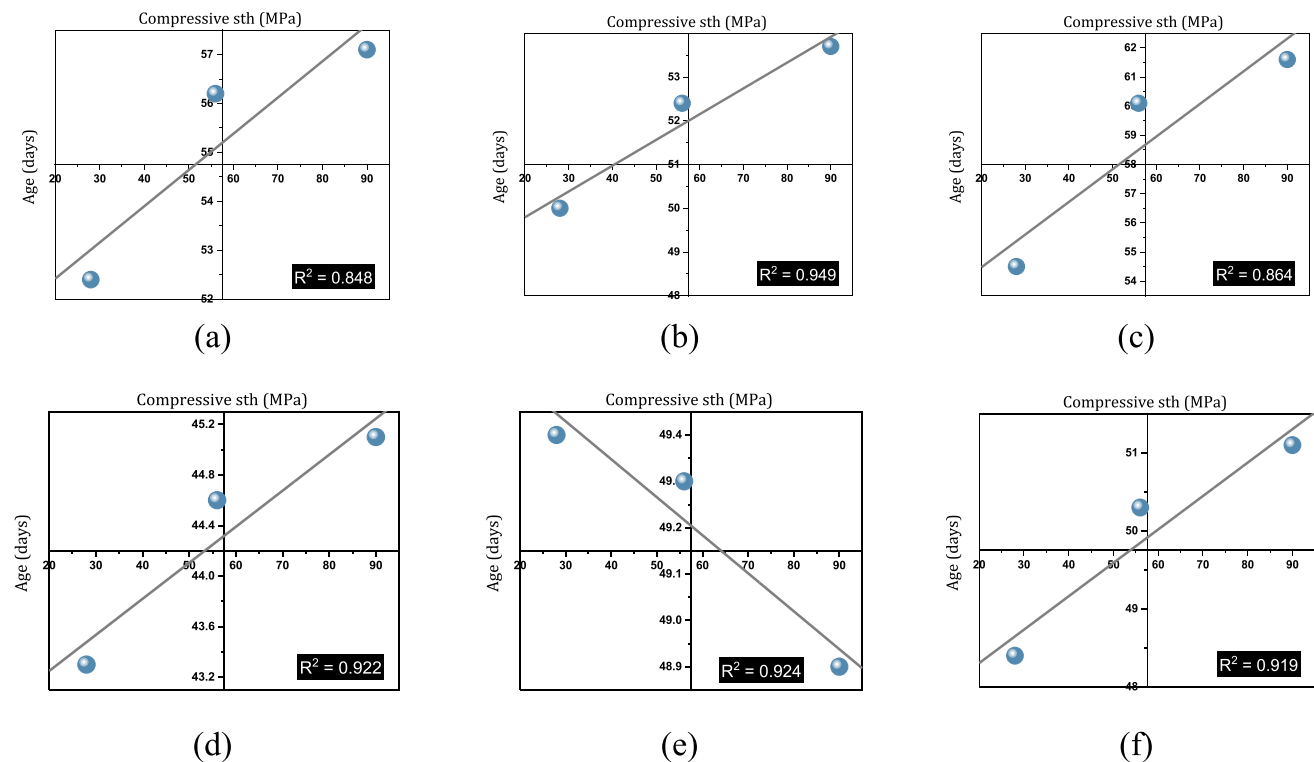
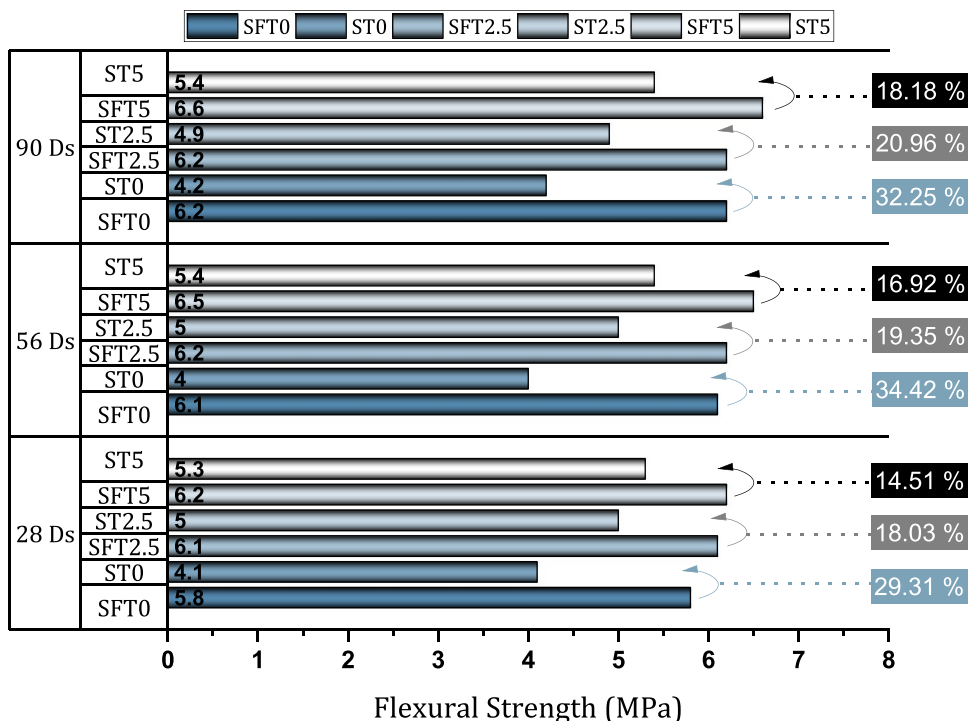


Fig. 9 Correlation between compressive strength results of different ages: **a** SFT0, **b** SFT2.5, **c** SFT5, **d** ST0, **e** ST2.5, **f** ST5

Fig. 10 Flexural strength results (28, 56, and 90 days)



Flexural strength

Figure 10 shows the flexural strength results of different mixtures at the ages of 28, 56, and 90 days. Examining the separate phase mixtures (SFT0 and ST0) shows that the mixtures containing SF have higher flexural strength than the mixtures containing nS. The flexural strength of the SFT0 mixture at the ages of 28, 56, and 90 days was 5.8, 6.1, and 6.2 MPa, respectively, and these values were reduced by 29.31%, 34.42%, and 32.25% for the ST0 mixtures, respectively. The mechanism of specimen failure under compression and flexural differs, and it is believed that the failure under a flexural force depends highly on the ITZ and capillary pores inside the cement matrix. Since the replacement value for nS even at the optimum percentage (experimentally obtained and utilized in mix designs based on compressive strength results) leads to the agglomeration of particles, lower results for mixtures containing nS are inevitable. Capillary pores around the agglomerated particles are vulnerable under flexural and can be a zone for microcrack formation. When subjected to flexural, the propagation of one crack can lead to the failure of the specimen, but the mechanism is different in the compression case, where the propagation of numerous microcracks eventually causes the failure. Thus, when cracks are formed around the agglomerated particles, the failure of the specimen occurs at lower loads. It is expected that when an optimum amount of nS replaces cement, the specimens experience higher flexural strength. On the other hand, 20% of the cement has been replaced with SF, which also can be

considered a high replacement percentage, but it seems that the addition of SF has led to the maximum density of the cement matrix and decreased the number and connectivity of the capillary pores to the minimum. The reactivity of silica fume particles that results in a dense microstructure and filler effect of these particles reduces the porosity and consequently increases flexural strength. Also, the capillary effect of the wall of the SF particles facilitates the distribution of moisture inside the matrix and enhances the hydration process, leading to fewer capillary pores. It is expected that, in higher replacement values of SF, the agglomeration phenomenon occurs and the flexural strength is negatively affected by the increase in porosity.

The addition of UFTiO₂ positively affected the flexural strength of both SF- and nS-containing specimens. At the age of 28 days, the increase in flexural strength for SFT2.5 and SFT5 mixtures (UFTiO₂ + SF) was 5.17% and 6.89%, respectively. In addition, the increase in flexural strength for ST2.5 and ST5 mixtures (UFTiO₂ + nS) was recorded as 21.95% and 29.26%, respectively. The increase in flexural strength as a result of UFTiO₂ addition is more significant in specimens containing nS, which can be attributed to the substantial increase in packing density in these specimens in the presence of UFTiO₂. Higher particle size of UFTiO₂ compared to nS particles fills the gap between nS and cement particle size which consequently increases packing density. Examining the trend of increasing strength from 28 to 56 days showed that no substantial increase is observed in the specimens containing nS, while the corresponding

specimens with SF replacement showed an average 4% increase. This is due to the difference in the reactivity rate of these particles. In the case of SF, the reactions last longer, and at 28 and 56 days, the specimens still gain strength. In the case of nS, however, the reaction between cement and silica particles occurs at early ages. At 90 days, no significant strength increase is observed, which indicates that the contribution of high reactive SCMs, such as SF and nS, to the strength gain is far more significant at early ages. Figure 11 shows the correlation between the compressive and flexural strength of all the mixtures. As is observed, a linear correlation can be fit to the values with high R -squared

values. This shows a relationship between flexural and compressive strength. However, complications in these correlations are sensible due to the difference between the influence of SF and nS.

Electrical resistivity

Figure 12 shows the electrical resistivity results of mixtures at different ages (14, 28, 56, and 90 days). Between 14 and 28 days, all the specimens experienced a substantial increase in electrical resistivity. For ST0, ST2.5, and ST5 mixtures, the increase in strength was recorded as 49.8%,

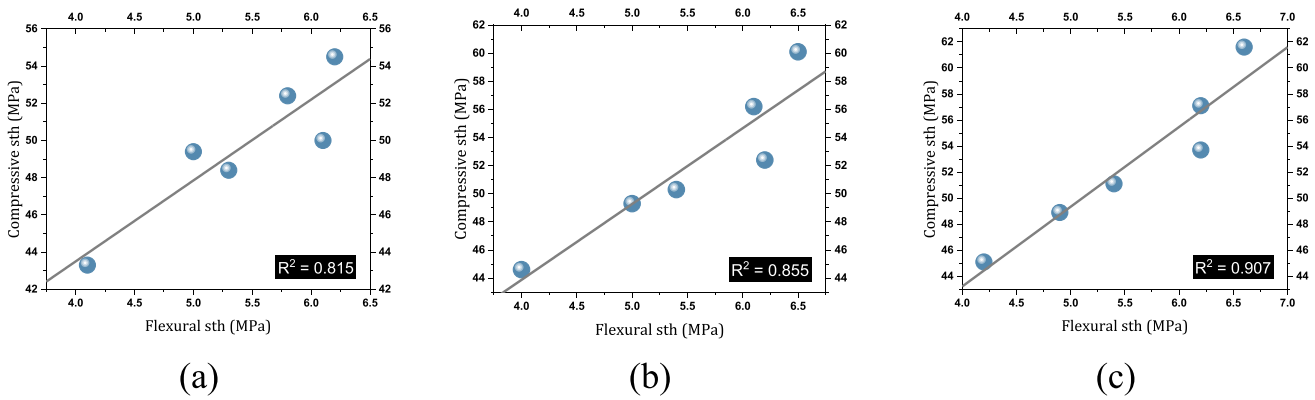
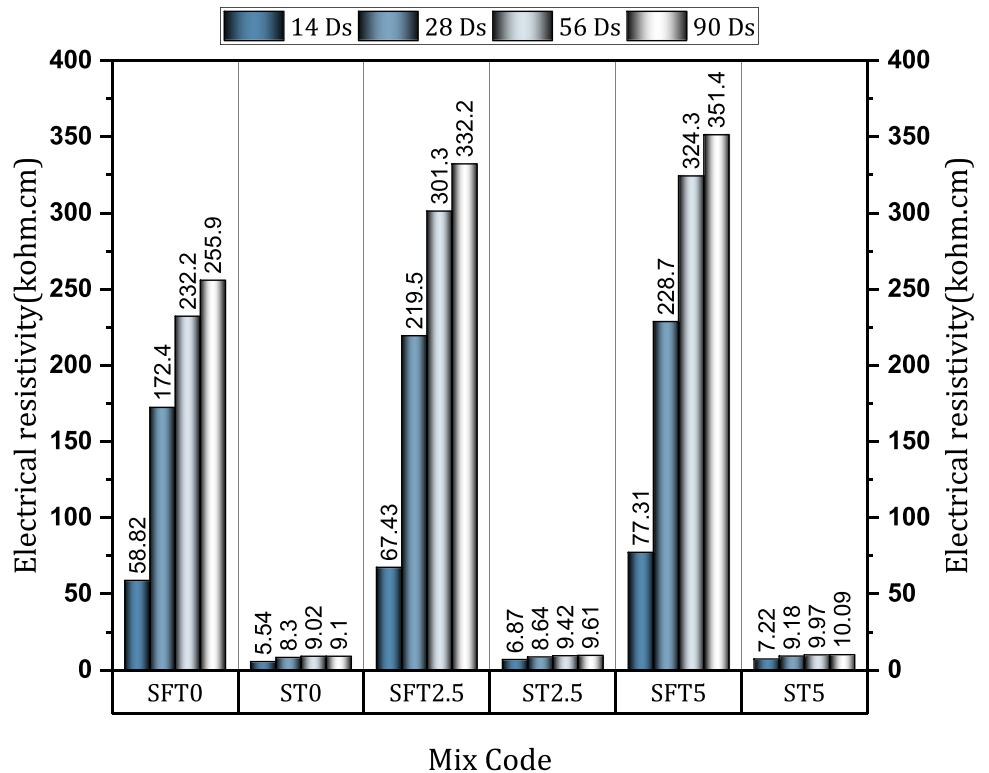


Fig. 11 Correlation between the compressive and flexural strength: **a** 28 days, **b** 56 days, **c** 90 days

Fig. 12 Electrical resistance results (28 days)



25.8%, and 27%, respectively. At early ages, due to the pozzolanic reactivity of nS, the dielectric phase of the matrix so-called C–S–H becomes denser, and the size and connectivity between capillary pores decreases; thus, an increase in electrical resistivity is observed. The connection of the pores plays a key role in the conductivity of cement composites. By evolving the hydration process, the connection between the pores is lost, and consequently, resistivity increases. Another noticeable point is that, by the addition of UFTiO₂, the resistivity has increased slightly. At the ages below 14 days, the surface of UFTiO₂ is a zone for the formation of Ca (OH)₂, which contributes to a higher electrical resistivity. This process of consolidation around UFTiO₂ particles probably depends on surface properties of these particles which facilitates the CSH formation and reorientation around aggregates and thus the closure of capillary pores. Thus, at later ages, the significance of UFTiO₂ is not as high as earlier. The difference between the values of 28 and 56 days is not significant. The completion of chemical reactions between nS and cement at early ages can be an explanation for this phenomenon. Beyond 56 days, no substantial increase is observed. Comparing the results, the mixtures containing UFTiO₂ (ST2.5 and ST5) exhibited higher electrical resistivity than the ST0. So compared to ST0, ST2.5 and ST5 mixtures showed an increase in electrical resistance by 24% and 30%, respectively.

Examining the mixture containing SF in Fig. 12 shows that the growth of resistance is significant until the age of 56 days, and after that the changes compared to the first 56 days period are insignificant. In this regard, for SFT0, SFT2.5, and SFT5 mixtures, the resistance was increased by 193%, 225%, and 196%, respectively. This increase is an indicator of the high pozzolanic reactivity of SF at this age. In fact, for up to 28 days, SF enters the pozzolanic reactions and

greatly increases the products of the hydration process. The pore refinement enabled by SF also reduces the connection and, at the same time, increases the tortuosity of the pore solution path inside the matrix. These phenomena lead to a great increase in the resistivity of the composite. From the age of 28 days to 56 days, the mixtures of SFT0, SFT2.5, and SFT5 experienced an increase in resistance by 34%, 37%, and 42%, respectively. This shows the reactivity of the silica fume at this age. Although the pozzolanic reactivity of SF is not comparable to that of the early ages, these fine particles still contribute to increasing the resistivity by making the matrix denser. Lacking space for C–S–H growth, it is likely that unreacted SF grains are exposed to hydrated or semi-hydrated cement grains in the early days and initiate pozzolanic reactions at later ages. Between 56 and 90 days, the increase in resistivity is much slower than the ages below 56 days. With the addition of UFTiO₂, an increase of 14.6% and 31.5% is observed for the specimens containing 2.5% and 5% UFTiO₂ (SFT2.5 and SFT5), compared to that of SFT0 (14 days curing). The increase in resistivity as a result of UFTiO₂ addition is more significant in the case of specimens containing nS. This can be due to the enhanced packing density of these specimens in the presence of UFTiO₂.

Comparing the electrical resistivity results of the mixture containing SF and nS in Fig. 12 indicates that the resistance of SF mixtures shows significantly higher results. The low resistivity of the specimens with nS can be attributed to the agglomeration of particles or the particles' poor size distribution. Although the addition of UFTiO₂ has enhanced the resistivity, compared to the values of SF specimens, this increase is inconsiderable. The low electrical resistivity of specimens containing nS can be further investigated. The presence of UFTiO₂ particles around the agglomerates of nS will improve the network of CSH by reducing the amount

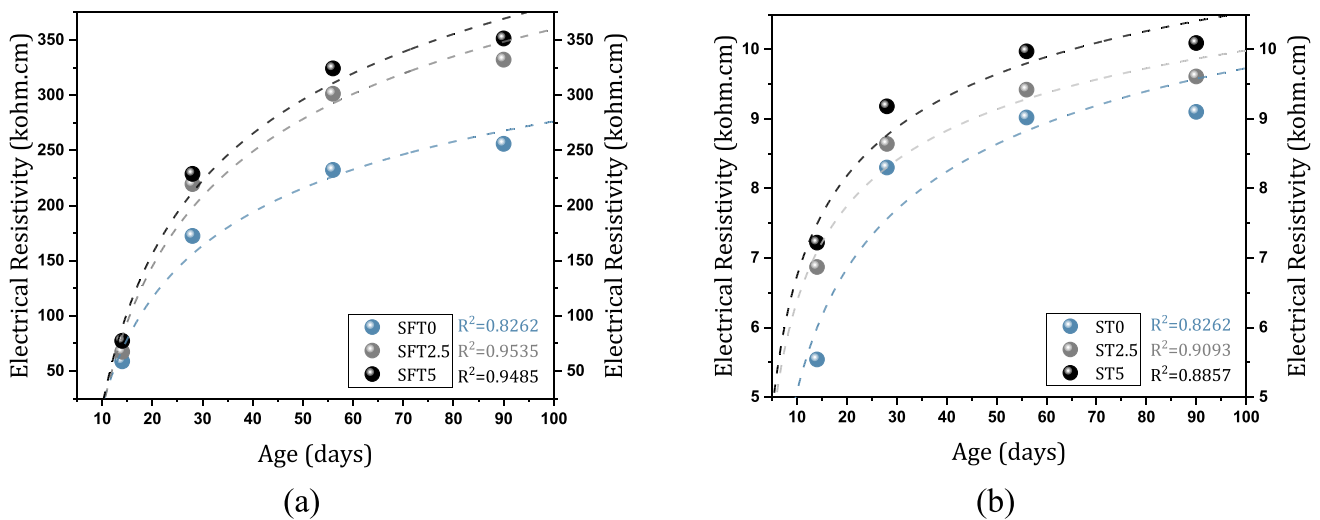


Fig. 13 Correlation between electrical resistivity results, a SFT, b ST

of free nS particles. On the other hand, the specimens containing SF showed high electrical resistivity due to the high pozzolanic reactivity, filler effect, and SF particle size distribution. From both Fig. 13a and b, there is a strong logarithmic correlation among the values. The trend of electrical resistance was accompanied by a significant increase at early ages, followed by a slow increase at ages beyond 28 days. It seems that at above 90 days, the curves will reach a plateau, perhaps due to the high pozzolanic activity of SF and nS, which make their contributions early. However, there are some practical implications which concern the water content that in industrial projects may vary substantially. So the rhythm of changing ER will change accordingly and new correlations will be required.

Abrasion resistance

Figure 14 shows the results of abrasion resistance test for different mixtures at the age of 28 days. Compared to the ST0 mixture, ST2.5 and ST5 mixtures (containing nS and UFTiO₂) recorded a 24% and 30% increase in mass loss, respectively. While the mass loss of ST0 is 176.6 g/m², the mass loss of ST2.5 and ST5 is 220 and 230 g/m², respectively. With regard to the initial weight of the specimens, 0.4% of the ST0 weight was abraded, while 0.5% and 0.57% of the weight of ST2.5 and ST5 were lost during the test. The decrease in abrasion resistance by adding UFTiO₂ can be attributed to the role of nanoparticles and ultra-fine TiO₂ particles. When an optimal amount of nS with a suitable size distribution is added, the empty space between the nanoparticles and the cement-laden nS becomes a likely zone for Ca(OH)₂ crystallization. The abrasion resistance increases by the growth of Ca(OH)₂ crystals. When the concentration of nS is high and the UFTiO₂ is added, the fine UFTiO₂

particles act as a filler and occupy the spaces between particles and minimize the empty space. This is followed by the growth of C–S–H as the main product of hydration, and the amount of Ca(OH)₂ is minimized. The growth of C–S–H, which has lower abrasion resistance compared to calcium hydroxide, results in a mass loss greater than the binary cement composite containing nS. On the other hand, the addition of UFTiO₂ has led to an increase in the abrasion resistance of the specimens containing SF. The SFT2.5 and SFT5 mix designs have shown a 51.5% and 31% decrease in mass loss compared to that of the SFT0. The mass loss of the specimens without UFTiO₂ (SFT0) was 173.3 g/m², while the two other specimens (SFT2.5 and SFT5) showed a mass loss of 83.3 and 120 g/m². The total abraded mass of the specimens with 0%, 2.5%, and 5% UFTiO₂ was 0.4%, 0.2%, and 0.28%, respectively. The role of UFTiO₂ is different in the mixtures containing SF. It seems that the surface of the UFTiO₂ particles is a zone for Ca(OH)₂ crystallization. In fact, in a dense cement matrix in the presence of SF, there is not enough space for crystal formation and the surface of the UFTiO₂ can provide for portlandite crystallization. The decrease in mass loss particularly for the surfaces containing UFTiO₂, which can be applied for self-cleaning purposes, indicates the less pollution of the environment due to erosion. Furthermore, higher stability of the surface among the self-cleaning ability justifies the use of such surfaces as pavement materials. The optimum packing regarding SF particle size distribution provides the CSH layers stronger bonds with UFTiO₂ particles, specially at the surface which leads to higher abrasion resistance. On the contrary, problems associated with nS lead to more unstable UFTiO₂ particles at the CSH matrix and consequently the surface of the composite which decreases the abrasion resistance.

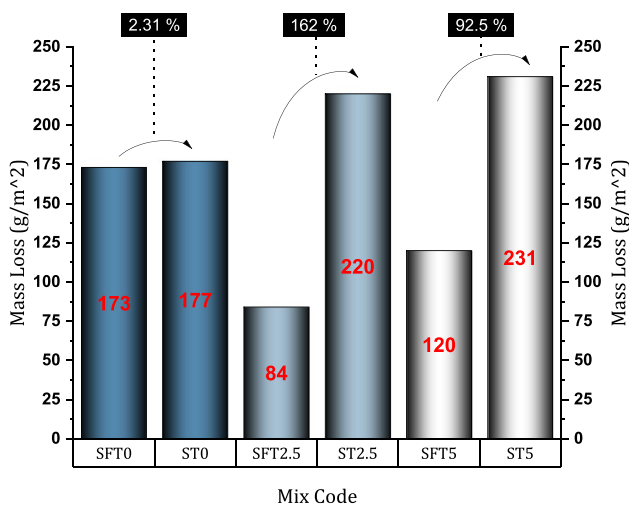


Fig. 14 The results of the abrasion resistance

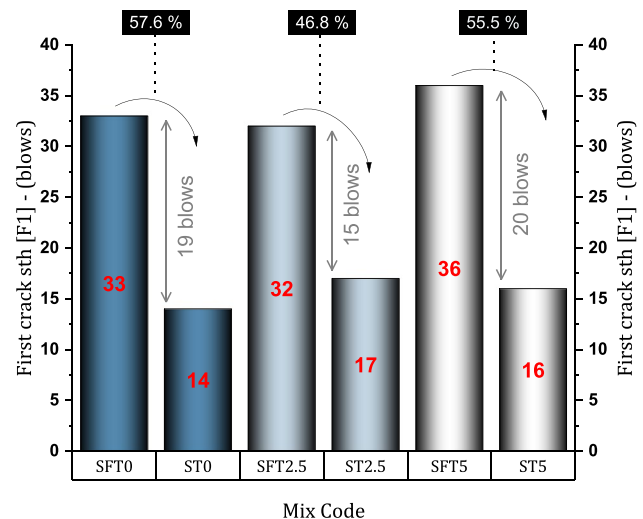


Fig. 15 Average first crack strength results

Impact strength (drop-weight test)

Figure 15 shows the results of the first crack strength of different mixtures. The SFT0 mixture has a first crack strength of 33 blows. Adding 2.5% and 5% of $UFTiO_2$ to the mixture containing SF (SFT2.5, SFT5) resulted in recording the first crack strength of 32 and 36 blows, respectively. Also, the mixture containing 3% nano-silica (ST0) shows the first crack strength of 14 blows. For ST2.5 and ST5 mixtures, the first crack strength of 17 and 16 blows was recorded, respectively. Comparing the mixtures of SFT (containing silica fume) and ST (without silica fume) shows that silica fume improves the resistance of the first crack by 88 to 135%. SFT5 mixture with 20% SF and 5% $UFTiO_2$ shows the best performance among other mixtures. Figure 16 shows the failure strength results of different mixes. The SFT mixtures containing 0% (SFT0), 2.5% (SFT2.5), and 5% (SFT5) $UFTiO_2$ obtained the failure strength of 39, 37, and 43 blows, respectively. For ST mixtures containing 0% (ST0), 2.5% (ST2.5), and 5% (ST5) $UFTiO_2$, 17, 21, and 21 blows were obtained, respectively. The comparison of SFT and ST mixtures shows the effect of using silica fume on failure strength so a 76 to 129% improvement in failure strength was achieved. Also, the combination of 20% silica fume and 5% $UFTiO_2$ (SFT5) showed the best results among the mixtures in terms of failure strength.

The impact strength of concrete depends on various factors, such as the type and amount of reinforcement, the curing conditions, the loading history, and the environmental exposure [113–115]. Silica fume, a very fine powder with a high content of silicon dioxide (SiO_2), improves the impact resistance of concrete by two main mechanisms: physical and chemical. The physical mechanism involves the particle size and shape of silica fume. The silica fume soot particles

are spherical and much smaller than the cement particles, so they can fill the gaps between them, lowering the porosity and permeability of concrete. This enhances the density and strength of concrete and makes it more resistant to cracking and spalling under impact load [116, 117]. The chemical mechanism involves the pozzolanic activity of silica fume. Silica fume reacts with calcium hydroxide ($Ca(OH)_2$), which is a by-product of cement hydration, and forms calcium silicate hydrate (C–S–H), which is the main phase of concrete bonding [118, 119]. This reaction decreases the amount of $Ca(OH)_2$, which is a weak and soluble compound, and increases the amount of C–S–H, which is a strong and insoluble compound. This improves the bond between the cement paste and the aggregates and enhances the cohesion and toughness of the concrete. The addition of $UFTiO_2$ has different effects in the mixture of nano-silica and silica fume [22, 64, 120]. $UFTiO_2$ may have a synergistic effect with nano-silica, as both of them can lower porosity and enhance concrete strength. $UFTiO_2$ may have a competitive effect with silica fume, as both of them can use up $Ca(OH)_2$ and influence the cement hydration process. In general, the effects of adding $UFTiO_2$ in mixtures with nano-silica and silica fume depend on factors such as synergistic effects, particle interaction, and optimal proportions.

Table 6 displays various statistical variables of the data derived from the first crack strength and failure strength of concrete mixtures. The coefficients of variation for mixtures containing SF are lower than those for mixtures containing nS. Based on the studies of Rahmani et al. [121] and Mohtsham Moin et al. [122], this implies that mixtures containing SF have less variability than mixtures containing nS. The 95% confidence interval values for different mixtures indicate the range of impact resistance with a 95% probability [121, 123]. The Kolmogorov–Smirnov test (K–S test) was applied to verify the normality of the impact test data. According to the K–S test, the *p* values for different mixtures, if they are less than 0.05, mean rejecting the null hypothesis of data normality [121, 123, 124]. The results show that the *p* values for the mixtures were higher than 0.15, which confirms the normality of the data.

Evaluating the first crack strength of concrete structures using tests such as the drop-weight test is essential for ensuring factors such as (1) structural integrity, (2) durability assessment, (3) design enhancement, and (4) quality control. By determining the first crack strength, engineers can design and construct concrete structures that can withstand anticipated loads and environmental conditions, while minimizing the occurrence of cracks and related issues. The first crack strength can be aligned with industry standards or specific requirements of a project in multiple ways. These include evaluating the project’s acceptance criteria, considering design factors, implementing quality control measures, adhering to performance-based specifications, and

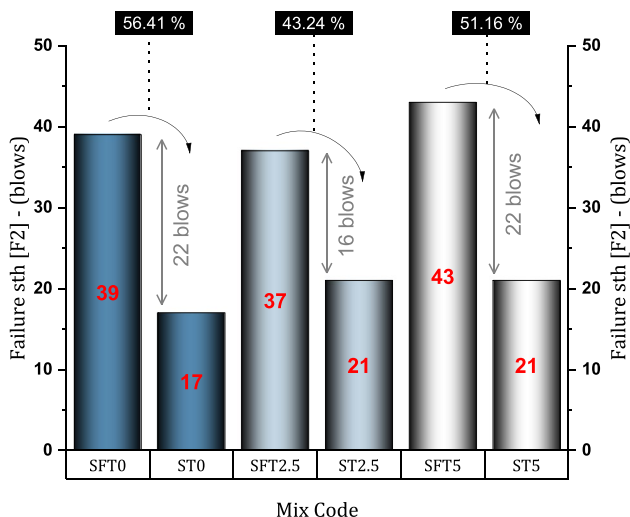


Fig. 16 Average failure strength results

Table 6 Statistical variables for first crack strength, failure strength

Mix code	Impact item	Mean (blows)	Standard Deviation (blows)	Coefficient of Variation (%)	95% Confidence Interval		The <i>p</i> -value of the K–S test
					Upper bound (blows)	Lower bound (blows)	
SFT0	First crack	33	5	16	29	36	> 0.15
SFT2.5		32	4	14	29	35	> 0.15
SFT5		36	4	10	33	38	> 0.15
NT0		14	3	24	11	16	0.128
NT2.5		17	4	22	15	20	> 0.15
NT5		16	3	20	14	18	> 0.15
SFT0	Failure	39	4	11	36	42	> 0.15
SFT2.5		37	4	12	34	40	> 0.15
SFT5		43	3	7	40	45	> 0.15
NT0		17	4	21	15	20	> 0.15
NT2.5		21	5	23	18	24	> 0.15
NT5		21	3	13	19	23	> 0.15

incorporating ongoing research and development efforts. The results obtained from drop-weight tests can provide insights into crack width, enabling engineers to design appropriate reinforcement and other measures to meet the required standards or specifications. Additionally, the drop-weight test can be utilized as part of quality control procedures during construction. In certain cases, project-specific requirements may rely on performance-based specifications rather than specific guidelines. In such instances, the first crack strength can serve as an indicator of performance, reflecting the structural behavior and durability of the concrete. It is important to note that correlations between the first crack strength determined from drop-weight testing and industry standards or project-specific requirements may be influenced by ongoing research and development activities. As new testing methods and performance-based criteria are developed, the interpretation and application of drop-weight test results may evolve to align with the latest advancements and industry practices.

The drop-weight test has several drawbacks. The test result can change considerably depending on the specimen characteristics, such as size, shape, notch depth, and bedding material [101, 115, 122, 125]. This means that the test conditions need to be very uniform and standardized to obtain reliable results [126]. This test requires a lot of specimens to get trustworthy results with a reasonable error margin. This makes testing expensive and time-consuming. This test does not consider the effects of strain rate, dynamic increase factor, and energy absorption capacity of concrete [126, 127]. These are the factors that affect the concrete behavior under impact loading in real scenarios. Therefore, some researchers [126–128] have proposed modifications to the ACI 544 test, such as using sand bedding, line notches, and different drop heights, to improve the accuracy and reliability of the

test. However, these modifications are not yet widely used or standardized.

Weibull distribution analysis of impact test

The drop-weight test recommended by the ACI 544 committee has a high dispersion of results, which has been confirmed by many researchers [121, 122, 125, 129]. Concrete and cement mortar have inherently brittle structures [130–133], which can be one reason for the dispersion of the drop-weight test. Therefore, the use of statistical methods in this field can be effective in providing better test results. In recent years, researchers have used several statistical techniques to analyze the results of concrete impact behavior. Statistical methods, such as the Kolmogorov–Smirnov test [121, 122], Kruskal–Wallis test [122], Ryan–Joiner test [134], Anderson–Darling test [134], and normal probability [135], have been widely used by researchers. Recently, the Weibull distribution has been considered to evaluate the behavior of concrete against impact. Wallodi Weibull [136] introduced this distribution in order to investigate the behavior of materials that have inherently brittle structures. In the field of the drop-weight test, Weibull distribution can be used to obtain the minimum safety impact resistance of concrete, which can be a practical tool for structural design [101, 137].

The Weibull function ($F(a)$) for the impact resistance distribution is according to Eq. (2), and the cumulative distribution function is according to Eq. (3) [101, 138]:

$$F(a) = \frac{\beta}{m - t_0} \left[\frac{t - t_0}{\gamma - t_0} \right]^{\beta-1} \exp \left\{ - \left[\frac{t - t_0}{\gamma - t_0} \right]^\gamma \right\} \quad (2)$$

$$F(b) = 1 - \exp \left\{ - \left[\frac{t - t_0}{\gamma - t_0} \right]^\beta \right\} \tag{3}$$

In Eq. (1), β represents the shape parameter, γ represents the scale parameter, and t_0 represents the location parameter, where $t \geq t_0, \beta > 0$, and $\gamma \geq t_0$. Equation (3) is summarized as follows, and Eq. (4) is obtained [137]:

$$S_N(a) = 1 - F(b) \tag{4}$$

where t_0 is considered zero for brittle composites [139, 140]. Hence, by modifying Eq. (5), Eq. (6) is given below [137]:

$$S_N(a) = \exp \left\{ - \left[\frac{t}{\gamma} \right]^\beta \right\} \tag{5}$$

The natural logarithm is taken from both sides of Eq. (5), and as a result, Eq. (6) is obtained [101]:

$$\ln \left[\ln \left(\frac{1}{S_N} \right) \right] = \beta \ln(t) - \beta \ln(\gamma) \tag{6}$$

According to Eq. (6):

$$Y = \ln \left[\ln \left(\frac{1}{S_N} \right) \right]$$

$$X = \beta \ln(t)$$

$$\varphi = \beta \ln(\gamma)$$

Finally, the linear regression equation is defined as follows [101]:

$$Y = \beta X - \varphi \tag{7}$$

Equation (7) presents the impact resistance by the two Weibull parameters. Using Eq. (7), it can be deduced whether the results of the drop-weight test (F1 and F2) follow the two-parameter Weibull function. The relationship between t and S_N is according to Eq. (8) [101]:

$$S_N = 1 - \frac{i - 0.3}{k + 0.4} \tag{8}$$

where i represents the number of concrete disks, and K represents the total number of concrete disks for each mix. Figures 17 and 18 show the graph between $\ln[\ln(1/S_N)]$ and $\ln(F1 \text{ or } F2)$ for the first crack strength and failure strength, respectively. The shape parameter (β), which is the slope of the line of the linear equation, is obtained through the output graphs (Figs. 17 and 18). The scale parameter (γ) is also obtained from Eq. (9) [101]:

$$\gamma = e^{(-\varphi/\beta)} \tag{9}$$

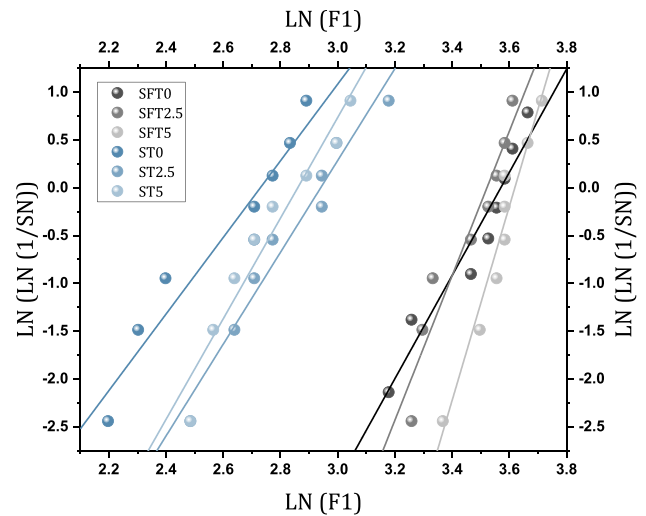


Fig. 17 Weibull lines of F1 from linear regression

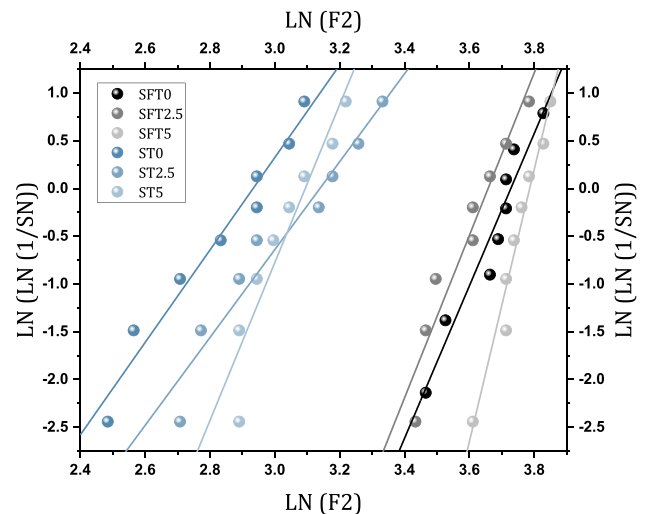


Fig. 18 Weibull lines of F2 from linear regression

Evaluation of impact resistance is done according to the required confidence levels through Eq. (10) [141]:

$$F_{1,2} = \gamma(-\ln(R_x))^{(1/\beta)} \tag{10}$$

Table 8 also shows the results of linear regression of different mixtures, which includes shape parameter (β), scale parameter (γ), intercept, and R^2 . By examining the results of Table 7 as well as Figs. 17 and 18, the linear distribution of the output data from the drop-weight test is obtained. To confirm this issue, the results of the coefficient of determination (R^2) output are used. The resulting R^2 value for different mixtures is about 0.9 and almost close to 1. Statistics experts believe that a reasonable model is a model with a detection coefficient of 0.7 or higher [121, 125].

Table 7 Weibull parameters

No	Mix code	Impact numbers	β	γ	ϕ	R^2
1	SFT0	F1	6.109	35.504	-21.775	0.938
2	SFT2.5		7.558	33.841	-26.617	0.925
3	SFT5		10.151	37.29	-36.735	0.944
4	ST0		4.008	15.329	-10.941	0.929
5	ST2.5		4.802	18.936	-14.123	0.962
6	ST5		5.263	17.467	-15.054	0.943
7	SFT0	F2	9.038	41.436	-33.659	0.941
8	SFT2.5		8.507	38.780	-31.118	0.941
9	SFT5		14.247	44.08	-53.94	0.963
10	ST0		4.841	18.758	-14.199	0.966
11	ST2.5		4.601	23.081	-14.444	0.945
12	ST5		8.268	22.064	-25.581	0.891

Under different levels of reliability, first crack strength and failure strength were evaluated by the Weibull distribution, the results of which are reported in Fig. 19. Based on the confidence level of 0.8, the F1 values for the mixtures SFT0, SFT2.5, SFT5, ST0, ST2.5, and ST5 were obtained as 27, 28, 32, 10, 14, and 13 blows, respectively. The F2 values for the confidence level of 0.8 were obtained for SFT0, SFT2.5, SFT5, ST0, ST2.5, and ST5 mixtures as 35, 32, 40, 14, 17, and 18 blows, respectively. The value of R^2 obtained from all mixtures is higher than 0.891; therefore, the impact resistance of mixtures containing nanomaterials can be evaluated from the proposed reliability curves with the required reliability. Scattered data from drop-weight tests can be analyzed by the Weibull distribution. Carrying out the drop-weight test requires significant money and time, but using the Weibull distribution can avoid these two factors and provide useful information to structural designers.

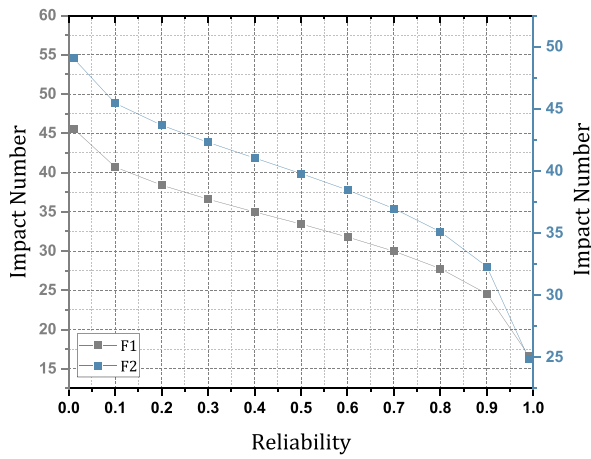
Previous studies [142–144] suggest that the Anderson–Darling statistical parameter is an appropriate criterion to assess the best fit among different models. Accordingly, a lower AD value for one model relative to other models indicates its superior fit [101, 137]. Figure 20 presents the AD values obtained from the impact data under normal, lognormal, and Weibull models for the first crack resistance and fracture resistance of concrete mixtures. The AD values demonstrate that the Weibull model outperforms the other two models. Table 8 provides a summary of other impact studies and their AD values. The findings of the current study are in line with those of other researchers reported in Table 8.

Microstructure analysis

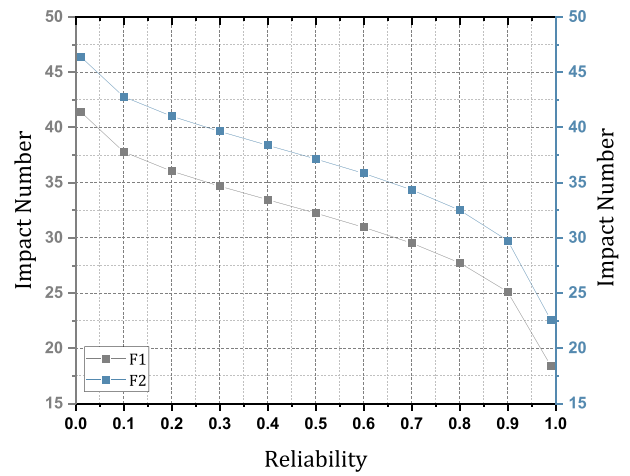
The hydration mechanism can differ greatly in the presence of supplementary cementitious materials, especially when highly reactive mineral admixtures such as silica fume

and nS are incorporated into the cement composites. During the first hours of hydration, the difference arises from a phenomenon called the filler effect, which includes two major factors. First, cement grains are replaced with very fine particles, and more space will thus be available for hydration products to grow. Second, the high surface area of these SCMs is a suitable space for hydrate precipitation [147]. In such cementitious systems, during the first hours of hydration, C–S–H needles grow outward from the surface of grains, and then, by fully occupying the surface, C–S–H growth undertakes a new pattern. A dense inner product is formed, which is responsible for the strength and density of the microstructure. This mechanism is observed in Fig. 21a, b, and c in the specimens containing nano-silica (nS). Note that the micrographs were taken at different stages of hydration. In the first stage (Fig. 21a), “sheaf of wheat”-shaped C–S–H is formed on the surface [148]; then, (Fig. 21b) the surface is occupied by needle-shaped C–S–H gel, and finally, a considerable growth in the density of C–S–H is observed as the inner product starts to grow (Fig. 21c).

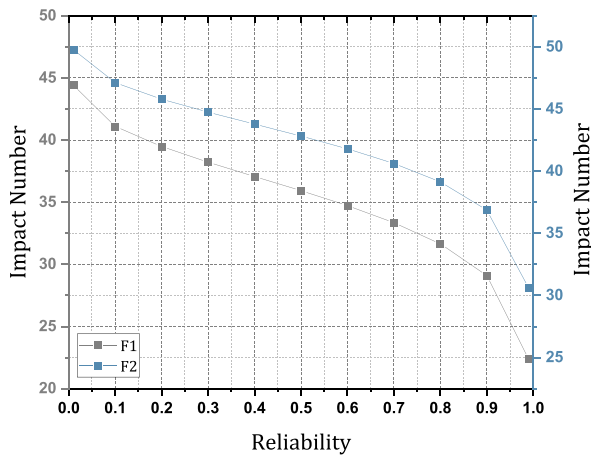
Beyond 1 day, it is believed that the hydration of different cementitious systems is similar to each other, and hence, no significant difference is observed in the microstructure. The relatively high reaction rate of SF and nS particles with portlandite, during the hydration of cement, accelerates the hydration rate and consolidation of cementitious matrix and the development of secondary reactions mostly happens inside the texture of CSH which probably is the main reason for difficulty in detection of morphologic changes after this period. The microstructural changes beyond 1 day are a subject for further research. It is reported that the water-to-cement ratio plays an extremely important role at this hydration stage for up to 6 days. Beyond 6 days, it is expected that hydration kinetics would be similar in different cementitious composites. Figure 22a and b shows the micrographs at 7 days; similar morphology is observed in



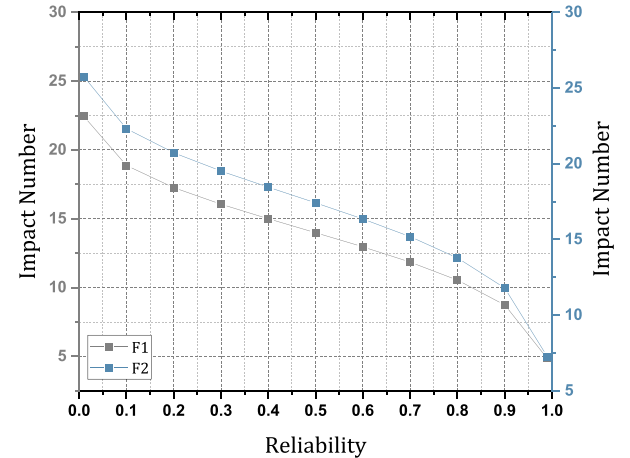
(a)



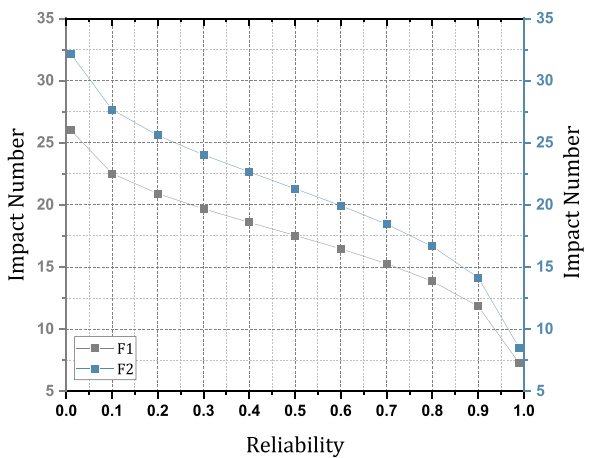
(b)



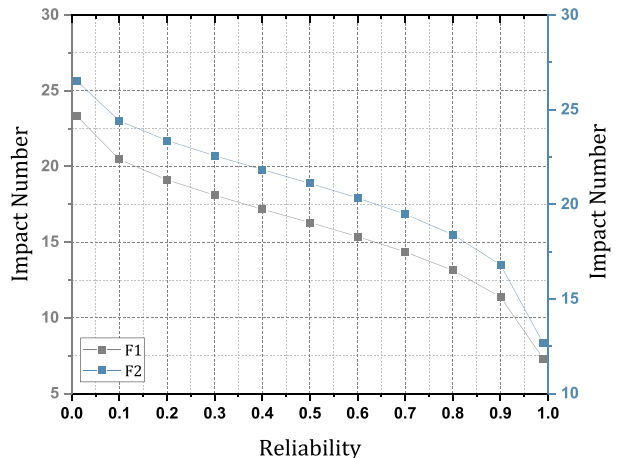
(c)



(d)



(e)



(f)

Fig. 19 Impact strength corresponding to reliability level: **a** SFT0, **b** SFT2.5, **c** SFT5, **d** ST0, **e** ST2.5, **f** ST5

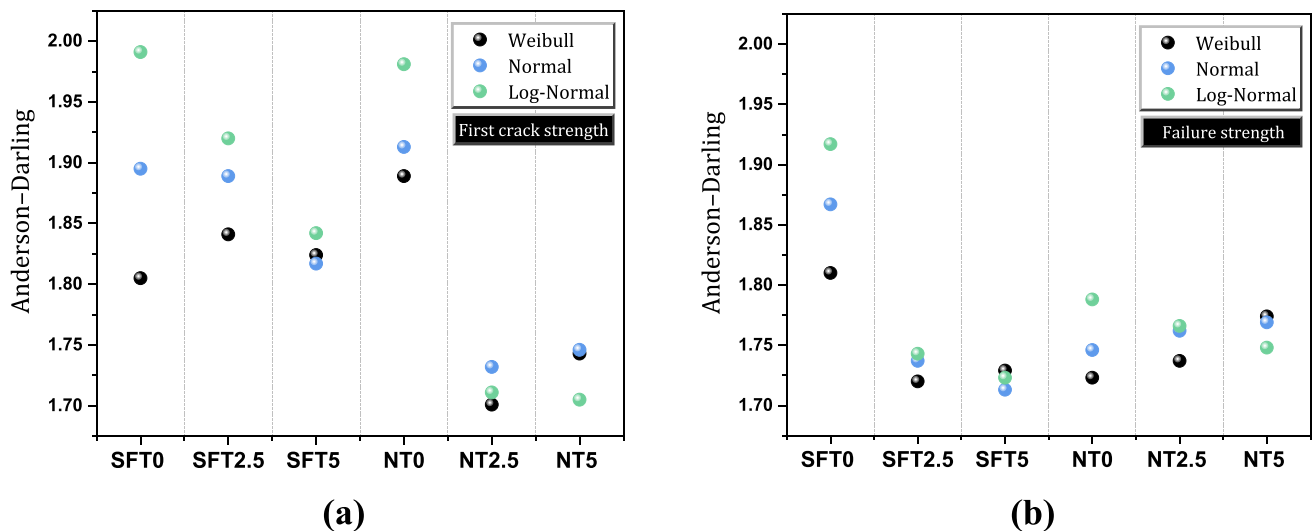


Fig. 20 Anderson–Darling results for normal, log-normal, and Weibull distributions: **a** first crack strength, **b** failure strength

specimens containing both SF and nS. This was expected according to the same water-to-cement ratio and similar chemical composition of SF and nS.

From the standpoint of mechanical strengths, the interfacial transition zone is the key factor in high-strength concrete. This issue becomes important when flexural strength is considered. In the field flexural test, the failure mechanism is based on the formation and propagation of a crack, which is more likely to occur in the ITZ. Different samples showed similar mechanical properties, so it is expected that the characteristics of the ITZ region will follow the same trend and many similarities will be found. Figure 23a shows the interfacial transition zone of the specimen containing silica fume (SF). There is a narrow microcrack at the interface, but the microcrack has not propagated into the cement paste. Figure 23b shows the interfacial transition zone of a specimen containing nano-silica (nS). A stronger zone is observed at some sections, but at the bottom of the figure, a microcrack with noticeable width is observed, and at the top of the figure, the microcrack is propagated into the cement paste. These could be the reasons for the lower mechanical strengths of specimens containing nS.

In terms of the substantial difference between the values of electrical resistivity, the most important factor is the capillary pores inside the cement matrix. When the density of the matrix decreases, the interconnected capillary pores grow and a direct path for the passing current becomes available. Figure 24a and b shows the cement matrix of specimens containing nano-silica (nS) and silica fume (SF), respectively. A denser and more uniform structure is observed in the case of the specimen with SF. In the specimen containing nS, the uniformity is not as sound as the other specimen and the density seems to be lower. Moreover, microcracks are seen,

which can decrease the electrical resistivity. These microcracks contribute to the pore structures such as capillary pores and absorb water and free ions which affect inversely the electrical resistivity and decrease mechanical strength of the composite.

UFTiO₂ particles provide space for the growth of hydration products, but according to the fineness of these particles, there are always potential problems pertaining to their agglomeration. Figure 25 shows the agglomerated UFTiO₂ particles. The hydrates are observed on the surface. The UFTiO₂ particles are about the same size, and this could negatively affect the microstructure. Particles with proper size distribution may more effectively contribute to enhancing the microstructure of the cement composites. It is noteworthy that this was the only zone with agglomerated UFTiO₂ particles. It seems that the hydration products have covered the surface of other UFTiO₂ particles, and they are not observed in the micrographs.

Conclusions

Compressive strength

- At all ages (28, 56, 90 days), the compressive strength of SF mixtures was higher than that of nS mixtures. While the compressive strength of the ST0 mixture at the ages of 28, 56, and 90 days was 43.4, 44.6, and 45.1 MPa, respectively, the SFT0 mixture obtained about 21% to 25% higher strength.
- Mixtures containing UFTiO₂ and SF (SFT2.5 and SFT5) result in higher compressive strength than UFTiO₂ and nS (ST2.5 and ST5). While the compressive strength of

Table 8 Weibull distribution results of other studies and Anderson–Darling

N:O	Refs.	Number of disks	Statistical method used	A–D test		Mix code	R ²	
				F1	F2		F1	F2
1	[101]	32	Weibull	W < N	W < N	Control, MS30-0.5, MS30-01, MS30-1.5, MM19-0.5, MM19-01, MM19-1.5, MM30-0.5, MM30-01, MM30-1.5, MM50-0.5, MM50-01, MM50-1.5	0.973, 0.9817, 0.9753, 0.9648, 0.991, 0.939, 0.8388, 0.9647, 0.9274, 0.9014, 0.9123, 0.943, 0.9133	0.9831, 0.9751, 0.9851, 0.9748, 0.976, 0.956, 0.8646, 0.9672, 0.9534, 0.9116, 0.9006, 0.9609, 0.8977
2	[145]	15	Weibull	W < N	W < N	CC, PAC1, PAC2, FG1, FG2, FG3, FG4, FG5, FG6, FG7, FG8, FG9	0.97, 0.88, 0.98, 0.84, 0.98, 0.98, 0.95, 0.92, 0.92, 0.94, 0.97, 0.99	0.99, 0.99, 0.97, 0.98, 0.97, 0.99, 0.99, 0.98, 0.99, 0.99, 0.91, 0.98
3	[137]	12	Weibull	W < N	W < N	SCCT0, SCCT25, SCCT50, SCCT75, SCCT100	0.9543, 0.9705, 0.9323, 0.8998, 0.8869	0.9742, 0.9794, 0.9147, 0.916, 0.8793
4	[146]	6	Weibull	W < N	W < N	RC, FC-50-1, FC75-1, FC-100-1, FC-125-1, FC-150-1, FC-50-2, FC-75-2, FC-100-2, FC-125-2, FC-150-2	0.95, 0.98, 0.96, 0.97, 0.97, 0.96, 0.98, 0.98, 0.98, 0.95, 0.94, 0.97, 0.99, 0.98, 0.95, 0.97, 0.98, 0.97, 0.93	0.98, 0.97, 0.93
5	[141]	6	Weibull	W < N	W < N	PC, PC-M, LF1, LF1-M, LF2, LF2-M, LF4, LF4-M	0.95, 0.94, 0.96, 0.92, 0.95, 0.92, 0.96, 0.98, 0.94, 0.92	0.98, 0.96, 0.96, 0.96, 0.95, 0.95, 0.97, 0.97, 0.97, 0.98, 0.94

A-D: Anderson–Darling test, W: Weibull, N: Normal

the ST2.5 mixture at the age of 28–90 days shows resistance in the range of 49–50 MPa, for the SFT2.5 mixture, it was about 1.5–10% higher.

- The addition of UFTiO₂ to the sample containing SF led to a slight increase in compressive strength (4–7%), but a more significant increase was recorded in the samples containing nS (8–14%).
- The larger particle size of SF compared to nS results in hydration progressing for longer periods. While nS mixtures usually reach their final strength at the age of 28 days, this behavior occurs for the mixtures containing SF at 56 days.

Flexural strength:

- The flexural strength of the ST0 mixture at the age of 28–90 days shows the range of 4–4.2 MPa. Meanwhile, for the SFT0 mixture, this resistance range was about 42–52% higher.
- The flexural strength of mixtures containing UFTiO₂ and SF (SFT2.5 and SFT5) provides approximately 16% to 25% higher flexural strength than the mixtures containing UFTiO₂ and nS (ST2.5 and ST5).
- While the addition of UFTiO₂ to the sample containing SF (SFT2.5 and SFT5) resulted in an increase in flexural strength of 1–7%, for samples containing nS (ST2.5 and ST5) it was recorded at 16.5–35%.
- The percentage increase in strength of mixtures under the effect of curing age showed that from 28 to 56 days, there was no significant increase in mixtures containing nS, but for mixtures containing SF, an average increase of 4% was recorded.

Electrical resistance:

- The electrical resistance of the SFT0 mixture at the age of 14–90 days shows a range of 59–226 kohm.cm, but for the ST0 mixture, this range was 90–96% lower. This significant difference was also maintained for SFT2.5/ST2.5 and SFT5/ST5 mixtures.
- The growth of resistance from the age of 14 to 28 days was recorded for mixtures containing nS in the range of 25–50%, but for mixtures containing SF, an increase of 193–225% was obtained.
- The addition of UFTiO₂ to the sample containing nS led to an increase in electrical resistance by 24–30% at the age of 14 days, but for the sample containing SF, this increase was in the range of 14.5–31.5%.

Abrasion resistance:

- ST0 mixture (contains only nS) compared to SFT0 mixture (contains only SF) results in about 2% more mass

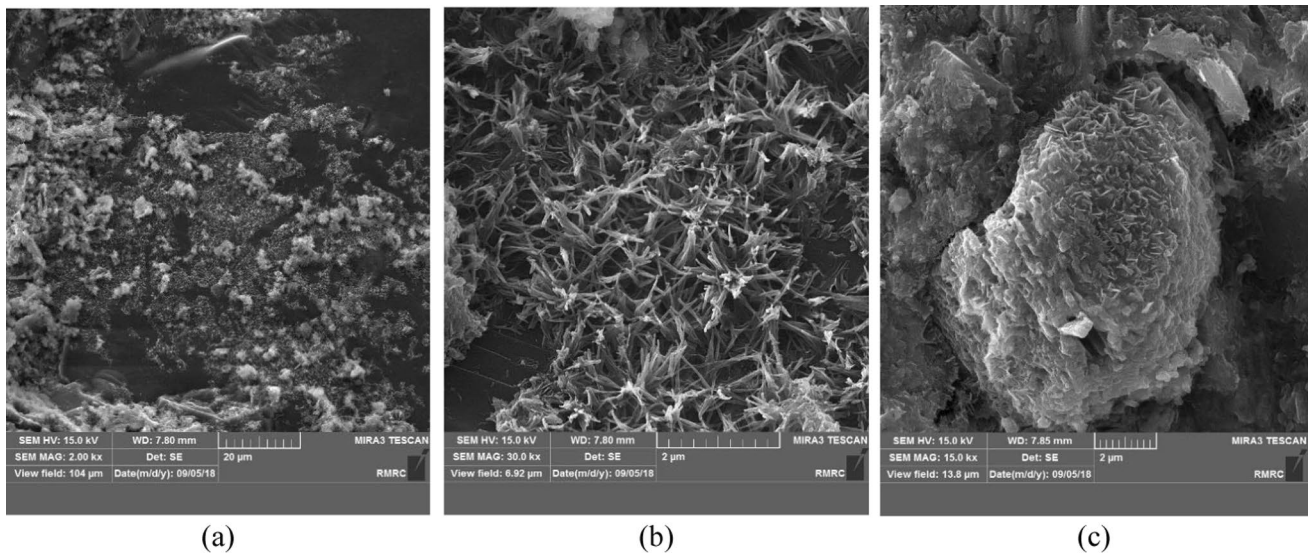


Fig. 21 Formation and reshaping of CSH structure during the aging process of cement matrix in **a** 7 days, **b** 28 days, **c** 90 days

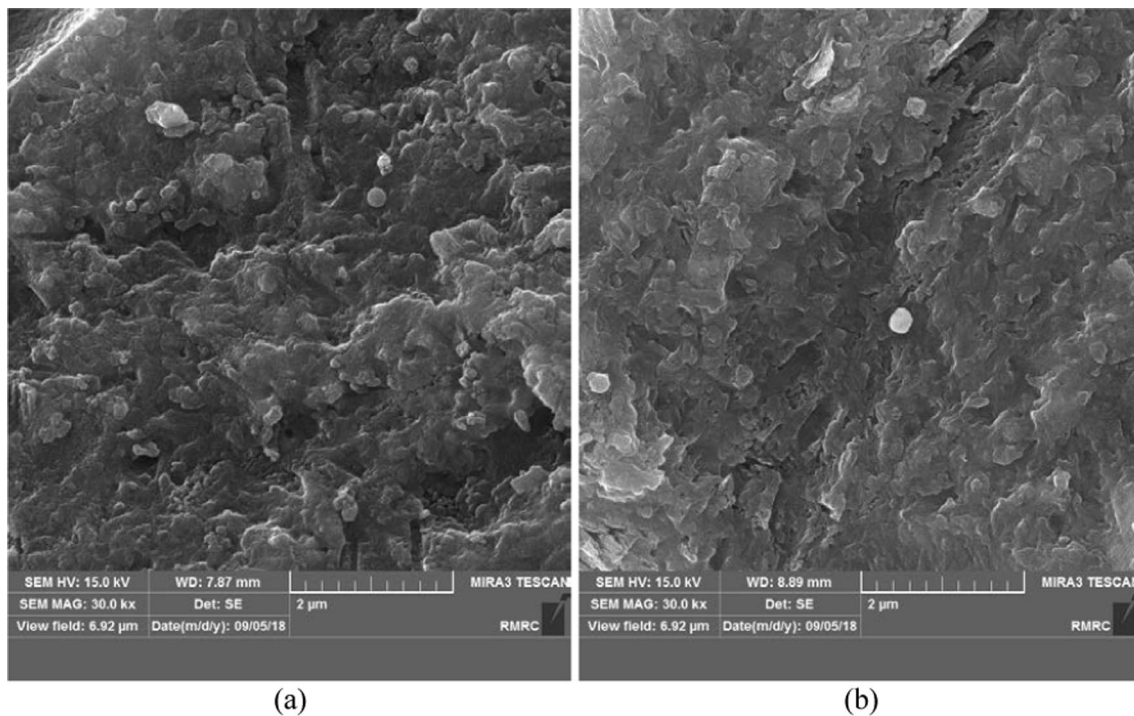


Fig. 22 Intact particles of **a** silica fume and **b** nano-silica in cement matrix

loss. A comparison of mixtures containing UFTiO_2 shows a stronger difference.

- The use of UFTiO_2 in mixtures containing SF resulted in improved abrasion resistance, but not in the case of mixtures containing nS.
- The amount of mass loss for the SFT2.5 and SFT5 mixtures was reduced by 51.5% and 31%, respectively, compared to the SFT0 mixture.

Impact resistance:

- The impact resistance of mixtures containing SF gave better results than mixtures containing nS. The strength of the first crack for SFT0, SFT2.5, and SFT5 mixtures was 33, 32, and 36 blows, respectively. (These values were reduced by 46% to 57% for mixtures containing Ns.) The failure strength for SFT0, SFT2.5, and SFT5

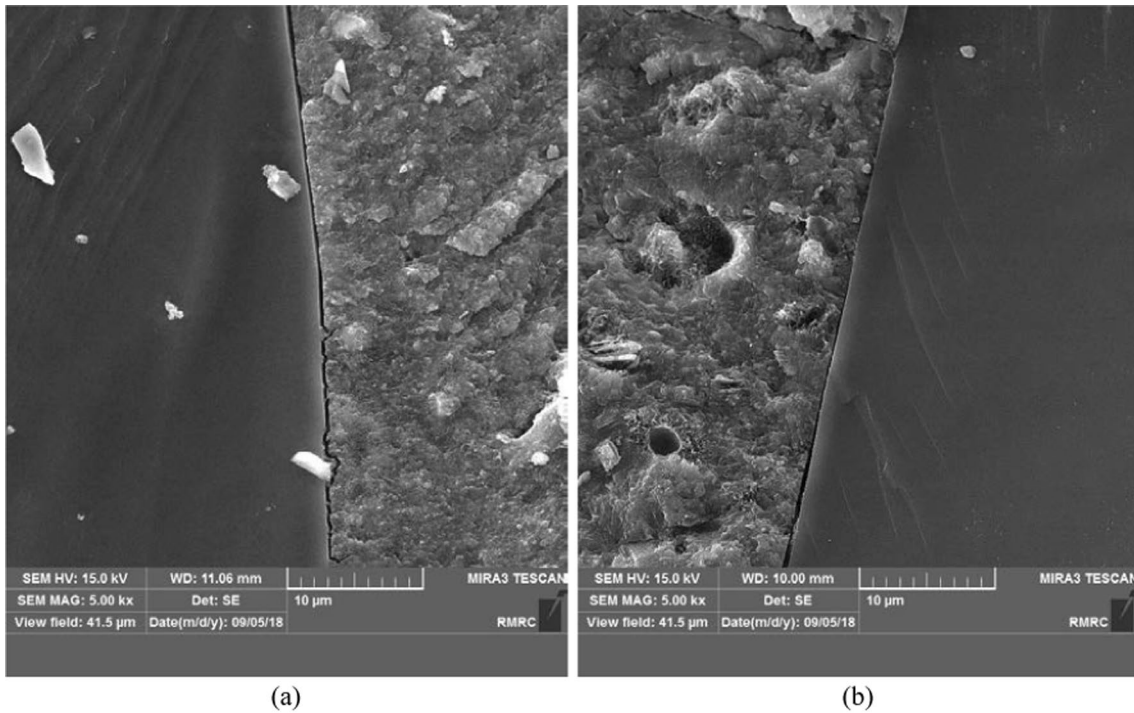


Fig. 23 ITZ gap between aggregate and cement matrix containing: **a** silica fume, **b** nano-silica

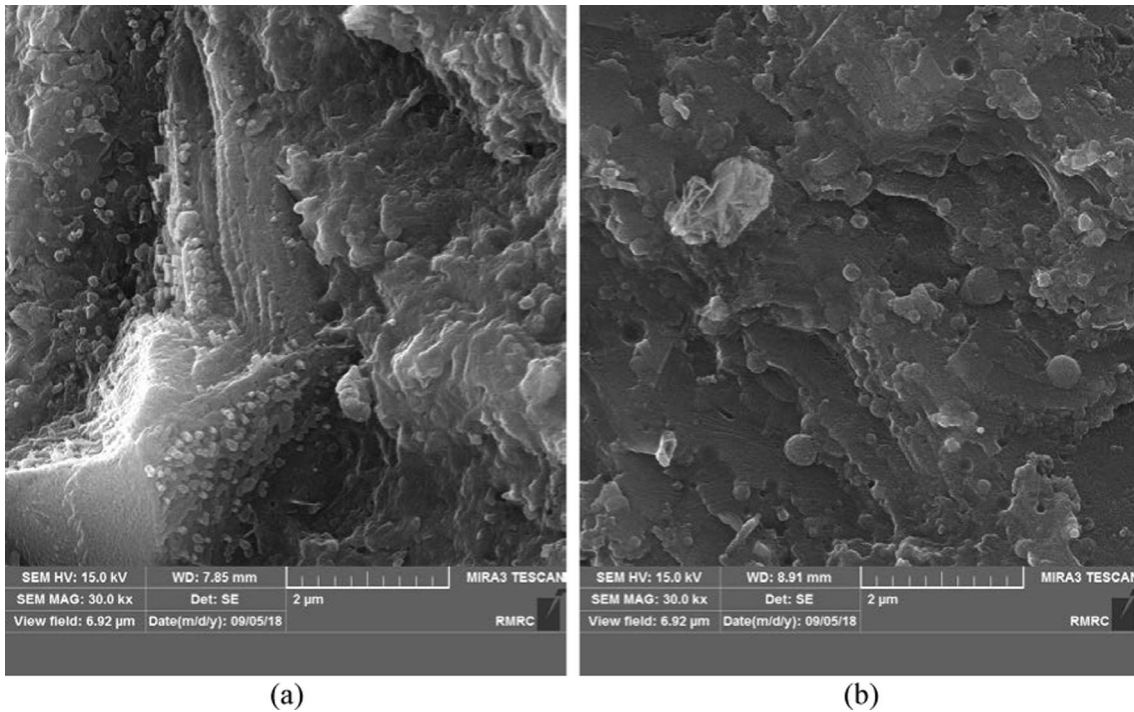


Fig. 24 Cement matrix containing at 90 days containing: **a** silica fume, **b** nano-silica

mixtures was 39, 37, and 43 blows, respectively. (These values were reduced by 43% to 56.5% for mixtures containing nS.)

- The investigation of Weibull distribution parameters shows the favorable results of this distribution for the impact strength of mixtures containing nanomaterials.

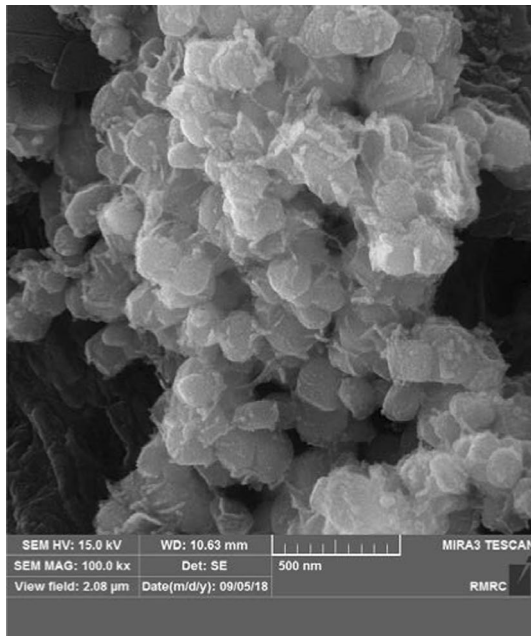


Fig. 25 Agglomeration of UFTiO₂ inside cement matrix

In addition, the presented graph of impact resistance-reliability can be a practical tool for designers.

Industrial perspective

Cement composites with enhancing additives as functional materials can play a pivotal role in modern construction industries such as precast elements of bridges or panels on facades of buildings due to advantages like considerably reduced weight of the members and elevated service life. Besides the environmental benefits of complex and reduced cement binding materials for composites in civil engineering, added values such as self-cleaning properties of the surface of CMs by using UFTiO₂ will justify the cost of these composites for urban applications specifically architectural goals.

Author contribution Ashkan Saradar contributed to methodology, validation, formal analysis, investigation, resources, data curation, writing—original draft, writing—review and editing, visualization, and supervision. Yousof Rezakhani was involved in validation, investigation, and resources and provided software. Komeil Rahmati contributed to writing—review and editing, and provided software. Farzad Johari Majd provided software and was involved in validation and formal analysis. Mohammad Mohtasham Moein contributed to conceptualization, methodology, validation, formal analysis, investigation, resources, data curation, writing—original draft, writing—review and editing, and visualization and provided software. Moses Karakouzian was involved in writing—review and editing, and visualization.

Funding This research received no external funding.

Data availability The data set analyzed during the current study is available and can be provided upon request.

Declarations

Conflict of interest The authors declare no conflict of interest.

Ethical approval Not applicable.

Informed consent Not applicable.

References

- Ramakrishna G, Sundararajan T (2005) Impact strength of a few natural fibre reinforced cement mortar slabs: a comparative study. *Cem Concr Compos*. <https://doi.org/10.1016/j.cemconcomp.2004.09.006>
- Safiuddin M, Abdel-Sayed G, Hearn N (2022) Flexural and impact behaviors of mortar composite including carbon fibers. *Materials*. <https://doi.org/10.3390/ma15051657>
- Shafiq P, Asadi I, Akhiani AR, Mahyuddin NB, Hashemi M (2020) Thermal properties of cement mortar with different mix proportions. *Mater de Constr*. <https://doi.org/10.3989/mc.2020.09219>
- Sadrumontazi A, Noorollahi Z, Tahmouresi B, Saradar A (2019) Effects of hauling time on self-consolidating mortars containing metakaolin and natural zeolite. *Constr Build Mater*. <https://doi.org/10.1016/j.conbuildmat.2019.06.037>
- Tajasosi S, Saradar A, Barandoust J, Mohtasham Moein M, Zeinali R, Karakouzian M (2023) Multi-criteria risk analysis of ultra-high performance concrete application in structures. *CivilEng* 4:1016–35. <https://doi.org/10.3390/civileng4030055>
- Husein I, Sivaraman R, Mohammad SH, Al-Khafaji FAH, Kadhim SI, Rezakhani Y (2024) Predictive equations for estimation of the slump of concrete using GEP and MARS methods. *J Soft Comput Civ Eng* 8:1–18. <https://doi.org/10.22115/scce.2023.389726.1619>
- Xuan D, Zhan B, Poon CS. Development of a new generation of eco-friendly concrete blocks by accelerated mineral carbonation. *J Clean Prod* 2016;133. doi <https://doi.org/10.1016/j.jclepro.2016.06.062>.
- Habert G, Denarié E, Šajna A, Rossi P (2013) Lowering the global warming impact of bridge rehabilitations by using ultra high performance fibre reinforced concretes. *Cem Concr Compos*. <https://doi.org/10.1016/j.cemconcomp.2012.11.008>
- Mohtasham Moein M, Saradar A, Rahmati K, Ghasemzadeh Mousavinejad SH, Bristow J, Aramali V et al (2023) Predictive models for concrete properties using machine learning and deep learning approaches: a review. *J Buil Eng*. <https://doi.org/10.1016/j.jobbe.2022.105444>
- Tahmouresi B, Nemati P, Asadi MA, Saradar A, Mohtasham MM (2021) Mechanical strength and microstructure of engineered cementitious composites: a new configuration for direct tensile strength, experimental and numerical analysis. *Constr Build Mater*. <https://doi.org/10.1016/j.conbuildmat.2020.121361>
- Mohammad Mohtasham Moein, Soliman A (2022) Predicting the compressive strength of alkali-activated concrete using various data mining methods. In: Canadian society of civil engineering annual conference, Springer Nature Singapore, p 317–26. https://doi.org/10.1007/978-981-19-1004-3_26.
- Mansoori A, Mohtasham Moein M, Mohseni E (2020) Effect of micro silica on fiber-reinforced self-compacting composites containing ceramic waste. *J Compos Mater*. <https://doi.org/10.1177/0021998320944570>

13. Pacheco-Torgal F, Jalali S, Labrincha J, John VM (2013) Eco-efficient concrete. Woodhead Publishing Limited, Swaston, pp 85–96. <https://doi.org/10.1533/9780857098993>
14. Du X, Li Y, Huangfu B, Si Z, Huang L, Wen L et al (2023) Modification mechanism of combined nanomaterials on high performance concrete and optimization of nanomaterial content. *J Build Eng*. <https://doi.org/10.1016/j.jobe.2022.105648>
15. Kishore K, Pandey A, Wagri NK, Saxena A, Patel J, Al-Fakih A (2023) Technological challenges in nanoparticle-modified geopolymer concrete: a comprehensive review on nanomaterial dispersion, characterization techniques and its mechanical properties. *Case Stud Constr Mater*. <https://doi.org/10.1016/j.cscm.2023.e02265>
16. Irshad MA, Sattar S, Nawaz R, Al-Hussain SA, Rizwan M, Bukhari A et al (2023) Enhancing chromium removal and recovery from industrial wastewater using sustainable and efficient nanomaterial: a review. *Ecotoxicol Environ Saf*. <https://doi.org/10.1016/j.ecoenv.2023.115231>
17. Feynman RP (2002) There's plenty of room at the bottom: an invitation to enter a new field of physics. *Handbook of Nanoscience, Engineering, and Technology*. <https://doi.org/10.1201/9781420040623-8>.
18. Feynman RP (1960) A plenty of room at the bottom. In: *The annual meeting of the American Physical Society at the California Institute of Technology (Caltech)*, vol 23, pp 22–36. <https://calteches.library.caltech.edu/47/2/1960Bottom.pdf>
19. Sharon M (2019) *History of nanotechnology: from prehistoric to modern times*. Wiley. <https://books.google.com/books?id=L5J3swEACAAJ>
20. Zhu W, Bartos PJM, Porro A (2004) Application of nanotechnology in construction Summary of a state-of-the-art report. *Mater Struct/Materiaux et Constr*. <https://doi.org/10.1617/14234>
21. Abhilash PP, Nayak DK, Sangoju B, Kumar R, Kumar V (2021) Effect of nano-silica in concrete; a review. *Constr Build Mater*. <https://doi.org/10.1016/j.conbuildmat.2021.122347>
22. Mohtasham Moein M, Rahmati K, Saradar A, Moon J, Karakouzian M (2024) A critical review examining the characteristics of modified concretes with different nanomaterials. *Materials* 17:409. <https://doi.org/10.3390/ma17020409>
23. Bastami M, Baghbadrani M, Aslani F (2014) Performance of nano-Silica modified high strength concrete at elevated temperatures. *Constr Build Mater*. <https://doi.org/10.1016/j.conbuildmat.2014.06.026>
24. Durgun MY, Atahan HN (2018) Strength, elastic and microstructural properties of SCCs' with colloidal nano silica addition. *Constr Build Mater*. <https://doi.org/10.1016/j.conbuildmat.2017.10.041>
25. Younis KH, Mustafa SM (2018) Feasibility of using nanoparticles of SiO₂ to improve the performance of recycled aggregate concrete. *Adv Mater Sci Eng*. <https://doi.org/10.1155/2018/1512830>
26. Erdem S, Hanbay S, Güler Z (2018) Micromechanical damage analysis and engineering performance of concrete with colloidal nano-silica and demolished concrete aggregates. *Constr Build Mater*. <https://doi.org/10.1016/j.conbuildmat.2018.03.197>
27. Quercia G, Brouwers HJH (2010) Application of nano-silica (nS) in concrete mixtures. In: *8th Fib PhD symposium in Kgs Lyngby, Denmark*.
28. de Abreu GB, Costa SMM, Gumieri AG, Calixto JMF, França FC, Silva C et al (2017) Mechanical properties and microstructure of high performance concrete containing stabilized nano-silica. *Revista Materia*. <https://doi.org/10.1590/S1517-707620170002.0156>
29. Ambikakumari Sanalkumar KU, Yang EH (2021) Self-cleaning performance of nano-TiO₂ modified metakaolin-based geopolymers. *Cem Concr Compos*. <https://doi.org/10.1016/j.cemconcomp.2020.103847>
30. Paul KK, Giri PK (2018) Plasmonic metal and semiconductor nanoparticle decorated TiO₂-based photocatalysts for solar light driven photocatalysis. *Encycl Interfacial Chem Surface Sci Electrochem*. <https://doi.org/10.1016/B978-0-12-409547-2.13176-2>
31. Shchelokova EA, Tyukavkina V, Tsyryatyeva A, Kasikov AG (2021) Synthesis and characterization of SiO₂-TiO₂ nanoparticles and their effect on the strength of self-cleaning cement composites. *Constr Build Mater*. <https://doi.org/10.1016/j.conbuildmat.2021.122769>
32. Chen J, Kou S, Poon C (2012) Hydration and properties of nano-TiO₂ blended cement composites. *Cem Concr Compos* 34:642–649. <https://doi.org/10.1016/j.cemconcomp.2012.02.009>
33. Bautista-Gutierrez KP, Herrera-May AL, Santamaria-López JM, Honorato-Moreno A, Zamora-Castro SA (2019) Recent progress in nanomaterials for modern concrete infrastructure: advantages and challenges. *Materials*. <https://doi.org/10.3390/ma12213548>
34. Bogue R (2014) Smart materials: a review of capabilities and applications. *Assem Autom*. <https://doi.org/10.1108/AA-10-2013-094>
35. Hanafizadeh P, Eshraghi J, Ahmadi P, Sattari A (2016) Evaluation and sizing of a CCHP system for a commercial and office buildings. *J Build Eng*. <https://doi.org/10.1016/j.jobe.2015.11.003>
36. Singh LP, Ali D, Sharma U (2016) Studies on optimization of silica nanoparticles dosage in cementitious system. *Cem Concr Compos*. <https://doi.org/10.1016/j.cemconcomp.2016.03.006>
37. Meng T, Ying K, Yang X, Hong Y (2021) Comparative study on mechanisms for improving mechanical properties and microstructure of cement paste modified by different types of nanomaterials. *Nanotechnol Rev*. <https://doi.org/10.1515/ntrev-2021-0027>
38. Kurihara R, Maruyama I (2016) Influences of nano-TiO₂ particles on alteration of microstructure of hardened cement. In: *Proceedings of the Japan concrete institute*, vol 38.
39. Akhtar MN, Jameel M, Ibrahim Z, Bunnori NM (2022) Incorporation of recycled aggregates and silica fume in concrete: an environmental savior—a systematic review. *J Market Res* 20:4525–4544. <https://doi.org/10.1016/j.jmrt.2022.09.021>
40. Siddique R (2011) Utilization of silica fume in concrete: review of hardened properties. *Resour Conserv Recycl*. <https://doi.org/10.1016/j.resconrec.2011.06.012>
41. Sadrmomtazi A, Tahmouresi B, Saradar A (2018) Effects of silica fume on mechanical strength and microstructure of basalt fiber reinforced cementitious composites (BFRCC). *Constr Build Mater*. <https://doi.org/10.1016/j.conbuildmat.2017.11.159>
42. Jahandari S, Mohammadi M, Rahmani A, Abolhasani M, Miraki H, Mohammadifar L et al (2021) Mechanical properties of recycled aggregate concretes containing silica fume and steel fibres. *Materials*. <https://doi.org/10.3390/ma14227065>
43. Saradar A, Nemati P, Paskiabi AS, Moein MM, Moez H, Vishki EH (2020) Prediction of mechanical properties of lightweight basalt fiber reinforced concrete containing silica fume and fly ash: experimental and numerical assessment. *J Build Eng*. <https://doi.org/10.1016/j.jobe.2020.101732>
44. Dalvand A, Ahmadi M (2021) Impact failure mechanism and mechanical characteristics of steel fiber reinforced self-compacting cementitious composites containing silica fume. *Eng Sci Technol Int J*. <https://doi.org/10.1016/j.jestech.2020.12.016>
45. Nabighods K, Saradar A, Mohtasham Moein M, Mirgozar Langaoudi MA, Byzyka J, Karakouzian M (2023) Evaluation of self-compacting concrete containing pozzolan (zeolite, metakaolin & silica fume) and polypropylene fiber against sulfate attacks with different PH: an experimental study. *Innov Infrastruct Solut* 9(1):5. <https://doi.org/10.1007/s41062-023-01309-0>

46. Ransinchung RNGD, Kumar B (2010) Investigations on pastes and mortars of ordinary portland cement admixed with wollastonite and microsilica. *J Mater Civ Eng*. [https://doi.org/10.1061/\(asce\)mt.1943-5533.0000019](https://doi.org/10.1061/(asce)mt.1943-5533.0000019)
47. Pillai UU, Anand KB (2019) Performance evaluation of polyurethane-nano silica modified cement mortar. *Mater Today Proc*. <https://doi.org/10.1016/j.matpr.2020.10.314>
48. Ramezani Pour AA, Sedighi S, Kazemian M, Ramezani Pour A (2020) Effect of micro silica and slag on the durability properties of mortars against accelerated carbonation and chloride ions attack. *AUT J Civ Eng* 4:411–22. <https://doi.org/10.22060/ajce.2020.15943.5565>
49. Yön MŞ, Arslan F, Karatas M, Benli A (2022) High-temperature and abrasion resistance of self-compacting mortars incorporating binary and ternary blends of silica fume and slag. *Constr Build Mater*. <https://doi.org/10.1016/j.conbuildmat.2022.129244>
50. Khan K, Ullah MF, Shahzada K, Amin MN, Bibi T, Wahab N et al (2020) Effective use of micro-silica extracted from rice husk ash for the production of high-performance and sustainable cement mortar. *Constr Build Mater*. <https://doi.org/10.1016/j.conbuildmat.2020.119589>
51. Li H, Xiao HG, Yuan J, Ou J (2004) Microstructure of cement mortar with nano-particles. *Compos B Eng*. [https://doi.org/10.1016/S1359-8368\(03\)00052-0](https://doi.org/10.1016/S1359-8368(03)00052-0)
52. Li H, Xiao H, gang O, Ping J (2004) A study on mechanical and pressure-sensitive properties of cement mortar with nanophase materials. *Cem Concr Res*. <https://doi.org/10.1016/j.cemconres.2003.08.025>
53. Ramezani Pour AA, Mortezaei M, Mirvalad S (2021) Synergistic effect of nano-silica and natural pozzolans on transport and mechanical properties of blended cement mortars. *J Build Eng*. <https://doi.org/10.1016/j.jobe.2021.102667>
54. Gesoglu M, Güneysi E, Asaad DS, Muhyaddin GF (2016) Properties of low binder ultra-high performance cementitious composites: comparison of nanosilica and microsilica. *Constr Build Mater*. <https://doi.org/10.1016/j.conbuildmat.2015.11.020>
55. Nili M, Ehsani A (2015) Investigating the effect of the cement paste and transition zone on strength development of concrete containing nanosilica and silica fume. *Mater Des*. <https://doi.org/10.1016/j.matdes.2015.03.024>
56. Zhang MH, Islam J (2012) Use of nano-silica to reduce setting time and increase early strength of concretes with high volumes of fly ash or slag. *Constr Build Mater*. <https://doi.org/10.1016/j.conbuildmat.2011.11.013>
57. Shih JY, Chang TP, Hsiao TC (2006) Effect of nanosilica on characterization of Portland cement composite. *Mater Sci Eng A*. <https://doi.org/10.1016/j.msea.2006.03.010>
58. Li G (2004) Properties of high-volume fly ash concrete incorporating nano-SiO₂. *Cem Concr Res*. <https://doi.org/10.1016/j.cemconres.2003.11.013>
59. Li H, Hua ZM, Ping OJ (2006) Abrasion resistance of concrete containing nano-particles for pavement. *Wear*. <https://doi.org/10.1016/j.wear.2005.08.006>
60. Li H, Xiao H, Guan X, Wang Z, Yu L (2014) Chloride diffusion in concrete containing nano-TiO₂ under coupled effect of scouring. *Compos B Eng*. <https://doi.org/10.1016/j.compositesb.2013.09.024>
61. Rao S, Silva P, de Brito J (2015) Experimental study of the mechanical properties and durability of self-compacting mortars with nano materials (SiO₂ and TiO₂). *Constr Build Mater*. <https://doi.org/10.1016/j.conbuildmat.2015.08.049>
62. Ying J, Zhou B, Xiao J (2017) Pore structure and chloride diffusivity of recycled aggregate concrete with nano-SiO₂ and nano-TiO₂. *Constr Build Mater*. <https://doi.org/10.1016/j.conbuildmat.2017.05.168>
63. Shekari AH, Razzaghi MS (2011) Influence of nano particles on durability and mechanical properties of high performance concrete. *Procedia Eng*. <https://doi.org/10.1016/j.proeng.2011.07.382>
64. Karthikeyan B, Dhinakaran G (2018) Influence of ultrafine TiO₂ and silica fume on performance of unreinforced and fiber reinforced concrete. *Constr Build Mater*. <https://doi.org/10.1016/j.conbuildmat.2017.11.133>
65. Madani H, Norouzifar MN, Rostami J (2018) The synergistic effect of pumice and silica fume on the durability and mechanical characteristics of eco-friendly concrete. *Constr Build Mater*. <https://doi.org/10.1016/j.conbuildmat.2018.04.070>
66. Pedro D, de Brito J, Evangelista L (2017) Evaluation of high-performance concrete with recycled aggregates: use of densified silica fume as cement replacement. *Constr Build Mater*. <https://doi.org/10.1016/j.conbuildmat.2017.05.007>
67. Mastali M, Dalvand A (2016) Use of silica fume and recycled steel fibers in self-compacting concrete (SCC). *Constr Build Mater* 125:196–209. <https://doi.org/10.1016/j.conbuildmat.2016.08.046>
68. Song HW, Pack SW, Nam SH, Jang JC, Saraswathy V (2010) Estimation of the permeability of silica fume cement concrete. *Constr Build Mater* 24:5. <https://doi.org/10.1016/j.conbuildmat.2009.08.033>
69. Ali B, Ahmed H, Qureshi LA, Kurda R, Hafez H, Mohammed H et al (2020) Enhancing the hardened properties of recycled concrete (RC) through synergistic incorporation of fiber reinforcement and silica fume. *Materials*. <https://doi.org/10.3390/ma13184112>
70. Lin WT, Huang R, Chang JJ, Lee CL (2009) Effect of silica fumes on the permeability of fiber cement composites. *J Chin Instit Eng Trans Chin Instit Eng Ser A/Chung-Kuo Kung Ch'eng Hsueh K'an*. <https://doi.org/10.1080/02533839.2009.9671535>
71. Singh S, Shintre D, Ransinchung RNGD, Kumar P (2018) Performance of fine RAP concrete containing flyash, silica fume, and bagasse ash. *J Mater Civ Eng*. [https://doi.org/10.1061/\(asce\)mt.1943-5533.0002408](https://doi.org/10.1061/(asce)mt.1943-5533.0002408)
72. Mazloom M, Ramezani Pour AA, Brooks JJ (2004) Effect of silica fume on mechanical properties of high-strength concrete. *Cem Concr Compos*. [https://doi.org/10.1016/S0958-9465\(03\)00017-9](https://doi.org/10.1016/S0958-9465(03)00017-9)
73. Tanyildizi H, Coskun A (2008) Performance of lightweight concrete with silica fume after high temperature. *Constr Build Mater*. <https://doi.org/10.1016/j.conbuildmat.2007.07.017>
74. Wu Z, Khayat KH, Shi C (2019) Changes in rheology and mechanical properties of ultra-high performance concrete with silica fume content. *Cem Concr Res*. <https://doi.org/10.1016/j.cemconres.2019.105786>
75. ASTM. ASTM C150 / C150M-19a Standard Specification for Portland Cement. Annual Book of ASTM Standards 2019.
76. C1240–15 (2015) A standard specification for silica fume used in cementitious mixtures, West Conshohocken. Pa
77. ASTM (2017) ASTM C778 standard specification for standard sand. ASTM (American Society for Testing and Materials)
78. ASTM C494 (2013) Standard specification for chemical admixtures for concrete. Annual Book of ASTM Standards 04
79. ASTM C109 (2020) ASTM C109 / C109M - 20b. Standard test method for compressive strength of hydraulic cement mortars (Using 2-in. or [50 mm] Cube Specimens). Annual Book of ASTM Standards 04.
80. Wang YS, Cho HK, Wang XY (2022) Mixture optimization of sustainable concrete with silica fume considering CO₂ emissions and cost. *Buildings*. <https://doi.org/10.3390/buildings12101580>
81. Ahmad J, Abid SR, Arbili MM, Majdi A, Hakamy A, Deifalla AF (2022) A review on sustainable concrete with the partially

- substitutions of silica fume as a cementitious material. Sustain (Switzerland). <https://doi.org/10.3390/su141912075>
82. Goel G, Sachdeva P, Chaudhary AK, Singh Y (2022) The use of nanomaterials in concrete: a review. *Mater Today Proc*. <https://doi.org/10.1016/j.matpr.2022.09.051>
 83. Janczarek M, Klapiszewski Ł, Jędrzejczak P, Klapiszewska I, Ślosarczyk A, Jesionowski T (2022) Progress of functionalized TiO₂-based nanomaterials in the construction industry: a comprehensive review. *Chem Eng J*. <https://doi.org/10.1016/j.cej.2021.132062>
 84. ASTM C348–21 (2021) Standard test method for flexural strength of hydraulic-cement mortars. ASTM International 04
 85. AASHTO (2015) AASHTO TP 119: Standard method of test for electrical resistivity of a concrete cylinder tested in a uniaxial resistance Test.
 86. Wen S, Chung DDL (2001) Electric polarization in carbon fiber-reinforced cement. *Cem Concr Res*. [https://doi.org/10.1016/S0008-8846\(00\)00382-3](https://doi.org/10.1016/S0008-8846(00)00382-3)
 87. Xie P, Gu P, Beaudoin JJ (1996) Electrical percolation phenomena in cement composites containing conductive fibres. *J Mater Sci*. <https://doi.org/10.1007/BF00352673>
 88. Cao J, Chung DDL (2004) Electric polarization and depolarization in cement-based materials, studied by apparent electrical resistance measurement. *Cem Concr Res*. <https://doi.org/10.1016/j.cemconres.2003.09.003>
 89. Chen B, Wu K, Yao W (2004) Conductivity of carbon fiber reinforced cement-based composites. *Cem Concr Compos*. [https://doi.org/10.1016/S0958-9465\(02\)00138-5](https://doi.org/10.1016/S0958-9465(02)00138-5)
 90. Han B, Ding S, Yu X (2015) Intrinsic self-sensing concrete and structures: a review. *Measure (Lond)*. <https://doi.org/10.1016/j.measurement.2014.09.048>
 91. Han B, Guan X, Ou J (2007) Electrode design, measuring method and data acquisition system of carbon fiber cement paste piezoresistive sensors. *Sens Actuators A Phys*. <https://doi.org/10.1016/j.sna.2006.08.003>
 92. ASTM (2017) ASTM C944–99: Standard test method for abrasion resistance of concrete or mortar surfaces by the rotating-cutter method
 93. Foglar M, Hajek R, Fladr J, Pachman J, Stoller J (2017) Full-scale experimental testing of the blast resistance of HPPRC and UHPFRC bridge decks. *Constr Build Mater*. <https://doi.org/10.1016/j.conbuildmat.2017.04.054>
 94. Yoo DY, Banthia N (2017) Mechanical and structural behaviors of ultra-high-performance fiber-reinforced concrete subjected to impact and blast. *Constr Build Mater*. <https://doi.org/10.1016/j.conbuildmat.2017.05.136>
 95. Xu S, Wu P, Li Q, Zhou F, Chen B (2021) Experimental investigation and numerical simulation on the blast resistance of reactive powder concrete subjected to blast by embedded explosive. *Cem Concr Compos*. <https://doi.org/10.1016/j.cemconcomp.2021.103989>
 96. Feng J, Gao X, Li J, Dong H, He Q, Liang J et al (2019) Penetration resistance of hybrid-fiber-reinforced high-strength concrete under projectile multi-impact. *Constr Build Mater*. <https://doi.org/10.1016/j.conbuildmat.2019.01.038>
 97. Mina AL, Petrou MF, Trezos KG (2021) Resistance of an optimized ultra-high performance fiber reinforced concrete to projectile impact. *Buildings*. <https://doi.org/10.3390/buildings11020063>
 98. Yu R, Van Beers L, Spiesz P, Brouwers HJH (2016) Impact resistance of a sustainable ultra-high performance fibre reinforced concrete (UHPFRC) under pendulum impact loadings. *Constr Build Mater*. <https://doi.org/10.1016/j.conbuildmat.2015.12.157>
 99. Ziada M, Erdem S, Tammam Y, Kara S, Lezcano RAG (2021) The effect of basalt fiber on mechanical, microstructural, and high-temperature properties of fly ash-based and basalt powder waste-filled sustainable geopolymer mortar. *Sustain (Switzerland)*. <https://doi.org/10.3390/su132212610>
 100. Ashraf MR, Akmal U, Khurram N, Aslam F, Deifalla AF (2022) Impact resistance of styrene-butadiene rubber (SBR) latex-modified fiber-reinforced concrete: the role of aggregate size. *Materials*. <https://doi.org/10.3390/ma15041283>
 101. Moein MM, Saradar A, Rahmati K, Rezakhani Y, Ashkan SA, Karakouzian M (2023) Reliability analysis and experimental investigation of impact resistance of concrete reinforced with polyolefin fiber in different shapes, lengths, and doses. *J Build Eng*. <https://doi.org/10.1016/j.jobbe.2023.106262>
 102. State-of-the-art report on fiber reinforced concrete (1996). ACI Committee 544 report 544, 1R-96. Detroit: American Concrete Institute. ACI Committee 544.
 103. Elkady HM, Yasien AM, Elfeky MS, Serag ME (2019) Assessment of mechanical strength of nano silica concrete (NSC) subjected to elevated temperatures. *J Struct Fire Eng*. <https://doi.org/10.1108/JSFE-10-2017-0041>
 104. Hendrix D, McKeon J, Wille K (2019) Behavior of colloidal nanosilica in an ultrahigh performance concrete environment using dynamic light scattering. *Materials*. <https://doi.org/10.3390/ma12121976>
 105. Kong D, Du X, Wei S, Zhang H, Yang Y, Shah SP (2012) Influence of nano-silica agglomeration on microstructure and properties of the hardened cement-based materials. *Constr Build Mater*. <https://doi.org/10.1016/j.conbuildmat.2012.08.006>
 106. Khaloo A, Mobini MH, Hosseini P (2016) Influence of different types of nano-SiO₂ particles on properties of high-performance concrete. *Constr Build Mater*. <https://doi.org/10.1016/j.conbuildmat.2016.03.041>
 107. Xu Z, Gao J, Zhou Z, Zhao Y, Chen X (2020) Hydration and microstructure of tricalcium silicate incorporating nano-TiO₂. *Constr Build Mater*. <https://doi.org/10.1016/j.conbuildmat.2020.120805>
 108. Feng D, Xie N, Gong C, Leng Z, Xiao H, Li H et al (2013) Portland cement paste modified by TiO₂ nanoparticles: a microstructure perspective. *Ind Eng Chem Res*. <https://doi.org/10.1021/ie4011595>
 109. Sun J, Cao X, Xu Z, Yu Z, Zhang Y, Hou G et al (2020) Contribution of core/shell TiO₂@SiO₂ nanoparticles to the hydration of Portland cement. *Constr Build Mater*. <https://doi.org/10.1016/j.conbuildmat.2019.117127>
 110. Wang X, Pan Z, Zhu C, Zhu H (2014) Reaction degree of silica fume and its effect on compressive strength of cement-silica fume blends. *J Wuhan Univ Technol Mater Sci Ed*. <https://doi.org/10.1007/s11595-014-0986-4>
 111. Bodt BA, Ostle B, Turner K, Hicks C, McElrath G (1997) Engineering statistics: the industrial experience. *Technometrics*. <https://doi.org/10.2307/1270788>
 112. Edwards LJ, Muller KE, Wolfinger RD, Qaqish BF, Schabenberger O (2008) An R² statistic for fixed effects in the linear mixed model. *Stat Med*. <https://doi.org/10.1002/sim.3429>
 113. Yoo DY, Banthia N (2019) Impact resistance of fiber-reinforced concrete—a review. *Cem Concr Compos*. <https://doi.org/10.1016/j.cemconcomp.2019.103389>
 114. Abid SR, Abdul Hussein ML, Ali SH, Kazem AF (2020) Suggested modified testing techniques to the ACI 544-R repeated drop-weight impact test. *Constr Build Mater*. <https://doi.org/10.1016/j.conbuildmat.2020.118321>
 115. Abid SR, Abdul-Hussein ML, Ayoob NS, Ali SH, Kadhum AL (2020) Repeated drop-weight impact tests on self-compacting concrete reinforced with micro-steel fiber. *Heliyon*. <https://doi.org/10.1016/j.heliyon.2020.e03198>

116. Li HL, Xu Y, Chen PY, Ge JJ, Wu F (2019) Impact energy consumption of high-volume rubber concrete with silica fume. *Adv Civ Eng*. <https://doi.org/10.1155/2019/1728762>
117. Siddique R (2011) Utilization of silica fume in concrete: review of hardened properties. *Resour Conserv Recycl* 55:923–932. <https://doi.org/10.1016/j.resconrec.2011.06.012>
118. Chishi AK, Gautam L (2023) Sustainable use of silica fume in green cement concrete production: a review. *Innov Infrastruct Solut*. <https://doi.org/10.1007/s41062-023-01164-z>
119. Lou Y, Khan K, Amin MN, Ahmad W, Deifalla AF, Ahmad A (2023) Performance characteristics of cementitious composites modified with silica fume: a systematic review. *Case Stud Constr Mater*. <https://doi.org/10.1016/j.cscm.2022.e01753>
120. Gupta S (2013) Application of silica fume and nanosilica in cement and concrete—a review. *J Today's Ideas Tomorrow's Technol*. <https://doi.org/10.15415/jotitt.2013.12006>
121. Rahmani T, Kiani B, Shekarchi M, Safari A (2012) Statistical and experimental analysis on the behavior of fiber reinforced concretes subjected to drop weight test. *Constr Build Mater* 37:360–369. <https://doi.org/10.1016/j.conbuildmat.2012.07.068>
122. Mohtasham Moein M, Saradar A, Rahmati K, Hatami Shirkouh A, Sadrinejad I, Aramali V et al (2022) Investigation of impact resistance of high-strength portland cement concrete containing steel fibers. *Cem Mater High Perform Concr* 15:1–30. <https://doi.org/10.3390/ma15207157>
123. Song PS, Wu JC, Hwang S, Sheu BC (2005) Assessment of statistical variations in impact resistance of high-strength concrete and high-strength steel fiber-reinforced concrete. *Cem Concr Res* 35:393–399. <https://doi.org/10.1016/j.cemconres.2004.07.021>
124. Mastali M, Dalvand A (2016) The impact resistance and mechanical properties of self-compacting concrete reinforced with recycled CFRP pieces. *Compos B Eng* 92:360–376. <https://doi.org/10.1016/j.compositesb.2016.01.046>
125. Rahmati K, Saradar A, Mohtasham Moein M, Sadrinejad I, Bristow J, Yavari A et al (2022) Evaluation of engineered cementitious composites (ECC) containing polyvinyl alcohol (PVA) fibers under compressive, direct tensile, and drop-weight test. *Multiscale Multidiscip Model Exper Design*. <https://doi.org/10.1007/s41939-022-00135-8>
126. Abid SR, Murali G, Ahmad J, Al-Ghasham TS, Vatin NI (2022) Repeated drop-weight impact testing of fibrous concrete: state-of-the-art literature review, analysis of results variation and test improvement suggestions. *Materials*. <https://doi.org/10.3390/ma15113948>
127. Badr A, Ashour AF (2005) Modified ACI drop-weight impact test for concrete. *ACI Mater J* 102:249–255
128. Myers JJ, Tinsley M (2013) Impact resistance of blast mitigation material using modified aci drop-weight impact test. *ACI Mater J*. <https://doi.org/10.14359/51685668>
129. Mohtasham Moein M, Mousavi SY, Madandoust R, Naser Saeid HNS (2019) The Impact resistance of steel fiber reinforcement concrete under different curing conditions: experimental and statistical analysis. *J Civ Environ Eng* 49(1):109–121
130. Koushkbaghi M, Alipour P, Tahmouresi B, Mohseni E, Saradar A, Sarker PK (2019) Influence of different monomer ratios and recycled concrete aggregate on mechanical properties and durability of geopolymer concretes. *Constr Build Mater* 205:519–528. <https://doi.org/10.1016/j.conbuildmat.2019.01.174>
131. Saradar A, Tahmouresi B, Mohseni E, Shadmani A (2018) Restrained shrinkage cracking of fiber-reinforced high-strength concrete. *Fibers*. <https://doi.org/10.3390/fib6010012>
132. Shadmani A, Tahmouresi B, Saradar A, Mohseni E (2018) Durability and microstructure properties of SBR-modified concrete containing recycled asphalt pavement. *Constr Build Mater*. <https://doi.org/10.1016/j.conbuildmat.2018.07.080>
133. Mosavinejad HG, Saradar A, Tahmouresi B (2018) Hoop stress-strain in fiber-reinforced cementitious composite thin-walled cylindrical shells. *J Mater Civ Eng* 30:1–12. [https://doi.org/10.1061/\(ASCE\)MT.1943-5533.0002428](https://doi.org/10.1061/(ASCE)MT.1943-5533.0002428)
134. Fakharifar M, Dalvand A, Arezoumandi M, Sharbatdar M, Chen G, Kheyroddin A (2014) Mechanical properties of high performance fiber reinforced cementitious composites. *Constr Build Mater* 71:510–520
135. Mastali A, Dalvand A, Sattarifard A (2016) The impact resistance and mechanical properties of reinforced self-compacting concrete with recycled glass fiber reinforced polymers. *J Clean Prod* 124:312–324
136. Weibull W (1939) A statistical theory of the strength of materials, vol 151. Generalstabens Litografiska Anstalts Förlag, Stockholm. <https://books.google.com/books?id=otVRAQAAIAAJ>
137. Mousavinejad SHG, Saradar A, Jabbari M, Moein MM (2023) Evaluation of fresh and hardened properties of self-compacting concrete containing different percentages of waste tiles. *J Build Pathol Rehabil*. <https://doi.org/10.1007/s41024-023-00329-8>
138. Murali G, Asrani NP, Ramkumar VR, Siva A, Haridharan MK (2019) Impact resistance and strength reliability of novel two-stage fibre-reinforced concrete. *Arab J Sci Eng*. <https://doi.org/10.1007/s13369-018-3466-x>
139. Haridharan MK, Matheswaran S, Murali G, Abid SR, Fediuk R, Mugahed Amran YH et al (2020) Impact response of two-layered grouted aggregate fibrous concrete composite under falling mass impact. *Constr Build Mater*. <https://doi.org/10.1016/j.conbuildmat.2020.120628>
140. Chen X, Liu Z, Guo S, Huang Y, Xu W (2019) Experimental study on fatigue properties of normal and rubberized self-compacting concrete under bending. *Constr Build Mater*. <https://doi.org/10.1016/j.conbuildmat.2019.01.207>
141. Murali G, Abid SR, Mugahed Amran YH, Abdelgader HS, Fediuk R, Susrutha A et al (2020) Impact performance of novel multi-layered prepacked aggregate fibrous composites under compression and bending. *Structures*. <https://doi.org/10.1016/j.istruc.2020.10.001>
142. Tumidajski PJ, Fiore L, Khodabocus T, Lachemi M, Pari R (2006) Comparison of Weibull and normal distributions for concrete compressive strengths. *Can J Civ Eng*. <https://doi.org/10.1139/L06-080>
143. Basu B, Tiwari D, Kundu D, Prasad R (2009) Is Weibull distribution the most appropriate statistical strength distribution for brittle materials? *Ceram Int*. <https://doi.org/10.1016/j.ceramint.2007.10.003>
144. Pedrosa B, Correia JAFO, Rebelo CAS, Veljkovic M (2020) Reliability of fatigue strength curves for riveted connections using normal and weibull distribution functions. *ASCE ASME J Risk Uncertain Eng Syst A Civ Eng*. <https://doi.org/10.1061/ajrua6.0001081>
145. Prasad N, Murali G (2021) Exploring the impact performance of functionally-graded preplaced aggregate concrete incorporating steel and polypropylene fibres. *J Build Eng*. <https://doi.org/10.1016/j.jobe.2020.102077>
146. Bilir L, Imir M, Yi D, Albostan A (2015) An investigation on wind energy potential and small scale wind turbine performance at Incek region-Ankara Turkey. *Energy Convers Manag*. <https://doi.org/10.1016/j.enconman.2015.07.017>

147. Scrivener KL, Juilland P, Monteiro PJM (2015) Advances in understanding hydration of Portland cement. *Cem Concr Res* 78:5. <https://doi.org/10.1016/j.cemconres.2015.05.025>
148. Juenger MCG, Monteiro PJM, Gartner EM, Denbeaux GP (2005) A soft X-ray microscope investigation into the effects of calcium chloride on tricalcium silicate hydration. *Cem Concr Res* 35:5. <https://doi.org/10.1016/j.cemconres.2004.05.016>

Springer Nature or its licensor (e.g. a society or other partner) holds exclusive rights to this article under a publishing agreement with the author(s) or other rightsholder(s); author self-archiving of the accepted manuscript version of this article is solely governed by the terms of such publishing agreement and applicable law.